Compensated isocurvature perturbations and the cosmic microwave background

Daniel Grin, Olivier Doré, and Marc Kamionkowski

Phys. Rev. D **84**, 123003 — Published 16 December 2011

DOI: 10.1103/PhysRevD.84.123003

Compensated Isocurvature Perturbations and the Cosmic Microwave Background

Daniel Grin[1], Olivier Doré[2,3], and Marc Kamionkowski[2]
[1] *School of Natural Sciences, Institute for Advanced Study, Princeton, NJ 08540*
[2] *California Institute of Technology, Mail Code 350-17, Pasadena, CA 91125 and*
[3] *Jet Propulsion Laboratory, California Institute of Technology, Pasadena, CA 91109*

Measurements of cosmic microwave background (CMB) anisotropies constrain isocurvature fluctuations between photons and non-relativistic particles to be sub-dominant to adiabatic fluctuations. Perturbations in the relative number densities of baryons and dark matter, however, are surprisingly poorly constrained. In fact, baryon-density perturbations of fairly large amplitude may exist if they are compensated by dark-matter perturbations, so that the total density remains unchanged. These compensated isocurvature perturbations (CIPs) leave no imprint on the CMB at observable scales, at linear order in their amplitude. B modes in the CMB polarization are generated at reionization through the modulation of the optical depth by CIPs, but this induced polarization is small. The strongest known constraint $\lesssim 10\%$ to the CIP amplitude comes from galaxy-cluster baryon fractions. Here it is shown that modulation of the baryon density by the CIP at and before the decoupling of Thomson scattering at $z \sim 1100$ gives rise to CMB effects several orders of magnitude larger than those considered before. Polarization B modes are induced, as are correlations between temperature/polarization spherical-harmonic coefficients of different lm. It is shown that the CIP field at the surface of last scatter can be measured with these higher-order correlations. The sensitivity of ongoing and future experiments to these fluctuations is estimated. Data from the WMAP, ACT, SPT, and Spider experiments will be sensitive to fluctuations with amplitude $\sim 5-10\%$. The Planck satellite and Polarbear experiment will be sensitive to fluctuations with amplitude $\sim 3\%$. SPTPol, ACTPol, and future space-based polarization methods will probe amplitudes as low as $\sim 0.4\% - 0.6\%$. In the cosmic variance limit, the lowest amplitude CIPs that could be detected with the CMB are of amplitude $\sim 0.05\%$.

PACS numbers: 98.70.Vc,95.35.+d,98.80.Cq,98.80.-k

I. INTRODUCTION

The concordance cosmological model posits a nearly scale-invariant spectrum of primordial density fluctuations with adiabatic initial conditions, for which the ratios of neutrino, photon, baryon, and dark-matter number densities are homogeneous. The simplest inflationary models predict adiabatic fluctuations [1–6], and adiabatic fluctuations are consistent with measurements of cosmic microwave background (CMB) temperature/polarization anisotropies [7] and the clustering of galaxies [8, 9].

Isocurvature perturbations are fluctuations in the ratios of number densities of various particle species. They are produced in topological-defect models for structure formation [10] and in more complicated models of inflation [11–16]. CMB temperature anisotropies limit the amplitude of baryon isocurvature perturbations (fluctuations in the baryon-to-photon ratio) [17, 18] and CDM isocurvature perturbations (fluctuations in the dark-matter–to–photon ratio) [19–22] to be $\lesssim 13\%$ of the total perturbation amplitude [7, 23–33].

Our intuition thus suggests the matter in the early Universe was very smoothly distributed. It therefore comes as somewhat of a surprise to learn that perturbations in the baryon density can be almost arbitrarily large, as long they are compensated by dark-matter perturbations such that the total-nonrelativistic-matter density remains unchanged [34, 35]. These compensated isocurvature perturbations (CIPs) thus obey

$$\rho_{\rm c}\delta_{\rm c}^{\rm CI} + \rho_{\rm b}\delta_{\rm b}^{\rm CI} = 0, \quad \delta_\gamma^{\rm CI} = 0, \tag{1}$$

where $\delta_{\rm c}$, $\delta_{\rm b}$, and δ_γ are fractional energy density perturbations in the dark matter, baryons, and photons, respectively, while $\rho_{\rm c}$ and $\rho_{\rm b}$ are the homogeneous dark matter and baryon densities.

CIPs induce no curvature perturbation at early times, and they therefore leave the photon density—and thus large-angle CMB fluctuations—homogeneous at linear order. CIPs induce baryon motion through baryon-pressure gradients, but these motions occur only at the baryon sound speed which, at the time when Thomson scattering first decouples ($z \sim 1100$, *decoupling* hereafter), is $(v/c) \sim (T/m_p)^{1/2} \sim ({\rm eV/GeV})^{1/2} \sim 10^{-4.5}$. The effects of these motions on CMB temperature and polarization anisotropies thus occur only on distances smaller than $\sim 10^{-4.5}$ times the sound horizon at decoupling or CMB multipole moments $l \sim 10^6$ [34, 36, 37], scales far smaller than those probed by CMB experiments.

The effect of CIPs on galaxy surveys is also small [34]. Big-bang nucleosynthesis (BBN) and galaxy-cluster baryon fractions constrain the CIP perturbation amplitude to be $\lesssim 10\%$ [35]. Measurements of fluctuations in 21-cm radiation from atomic hydrogen during the dark ages may be sensitive to these perturbations [34, 37–39], but these measurements are a long way in the future.

In Ref. [35], it was shown that although CIPs produce no observable effect on the CMB at linear order in per-

turbation theory, they modulate the CMB fluctuations produced by adiabatic perturbations. In particular, it was shown that B modes in the CMB polarization are produced by the angular modulation in the reionization optical depth induced by the CIP.

Here we consider the additional effects on CMB fluctuations that arise from modulation of the baryon density by CIPs at and before decoupling. CIPs modulate the free electron density. They thus change the photon diffusion length and thickness of the last scattering surface on different patches of sky. CIPs also change the weight of the baryon-photon plasma and thus the details of the acoustic-peak structure in the CMB power spectrum. Variation in the baryon density from one region on the sky to another thus leads to a modulation of the small-scale power spectrum from one region of sky to another. This induces B modes in the polarization and non-trivial higher-order correlations in the temperature/polarization map analogous to those induced by variations of other cosmological parameters [40] and those induced by weak gravitational lensing [41].

As we show below, the effects of CIPs on CMB fluctuations from decoupling are several orders of magnitude larger than those from reionization, and so the CMB should provide a far more sensitive probe of CIPs than envisioned in Ref. [35]. We therefore follow through and develop the formalism required to look for CIPs with the CMB. To do so, we write down the minimum-variance estimators that can be constructed from a CMB temperature-polarization map for the CIP field $\Delta(\hat{n})$ as a function of position $\hat{n}$ on the sky. We evaluate the noise with which the CIP field can be reconstructed and estimate the signal-to-noise with which a scale-invariant spectrum of CIPs may be detected with various experiments.

We conclude that data from WMAP, Spider, ACT, and SPT are sensitive to CIP amplitudes of $\sim 5-10\%$. The Planck satellite [42] and Polarbear experiment are sensitive to CIP amplitudes as small as $\sim 3\%$. Upcoming ground-based polarization experiments (ACTPol [43] and SPTPol [44, 45]), or a post-Planck CMB-polarization experiment along the lines of the proposed EPIC experiment [46] could detect fluctuations of $\sim 0.4\%-0.6\%$. In the cosmic variance limit, sensitivity to fluctuations of amplitude $\sim 0.05\%$ is possible.

Our principle motivation in studying CIPs is curiosity: can we determine empirically, rather simply assume, that the primordial baryon fraction is homogeneous and traces the dark matter? Still, there may be theoretical motivation as well. For example, curvaton models for inflation may generate CIPs [36, 47–49], with amplitudes approaching the regime detectable by EPIC [34]. It may also be that recent models [50–55] that connect the baryon asymmetry and dark-matter density have implications for CIPs.

In Ref. [56], we presented our basic conclusions. Here we present in detail our results, their derivation, and the computational methods used. We calculate the induced temperature anisotropies in Sec. II and the induced polarization anisotropies in Sec. III. In Sec. IV, we compute the expected corrections to CMB power spectra for a scale-invariant spectrum of CIPs and compare the B-mode power spectrum induced by CIPs at decoupling with that induced at reionization. In Sec. V, we construct minimum-variance estimators for CIPs. We then assess in Sec. VI the sensitivity of ongoing and upcoming experiments to CIPs, and we conclude in Sec. VII. Useful relations involving tensor spherical harmonics are presented in Appendix A. Numerical derivatives of transfer functions are discussed in Appendix B. Second-order harmonic expansions for CMB transfer functions are derived in Appendix C. Throughout we use as our fiducial cosmological parameters those from Ref. [7].

II. PERTURBED LINE-OF-SIGHT FORMALISM: TEMPERATURE

Here we review the standard calculation of the temperature-fluctuation power spectrum for primordial adiabatic density perturbations. We then show how this calculation is altered in the presence of CIPs.

A. General line-of-sight solution for temperature

The spherical-harmonic coefficients T_{lm} for the CMB temperature can be written,

$$\begin{aligned} T_{lm} &\equiv \int d\hat{n}\, T(\hat{n}) Y^*_{lm}(\hat{n}) \\ &= 4\pi \sum_{l_1 m_1} \int d\hat{n}\, Y^*_{lm}(\hat{n}) Y_{l_1 m_1}(\hat{n}) \int_0^{\eta_0} d\eta\, f(\eta,\hat{n}) \\ &\times \int \frac{d^3k}{(2\pi)^3} \Phi_{\vec{k}} i^{l_1} j_{l_1}[k(\eta_0-\eta)] Y^*_{l_1 m_1}(\hat{k}), \end{aligned} \tag{2}$$

where $T(\hat{n})$ is the CMB temperature in direction $\hat{n}$, and $Y_{lm}(\hat{n})$ are spherical harmonics. The Fourier transform of the primordial gravitational potential for wave-vector $\vec{k}$ is $\Phi_{\vec{k}}$, while $j_l(x)$ denotes a spherical Bessel function. The conformal time $\eta \equiv \int dt/a(t)$ is here an integration variable, and η_0 denotes its value today. The function $f(\eta,\hat{n})$, obtained via the numerical solution of the Boltzmann equations [57–59], encodes how much a real-space primordial potential perturbation $\Phi[(\eta-\eta_0)\hat{n},\eta]$ contributes to the temperature anisotropy $T(\hat{n})$. It depends on the relation between initial gravitational-potential fluctuations and radiation-density fluctuations at decoupling, as well as the recombination history.

B. Temperature anisotropies with homogeneous baryon fraction

In the standard calculation, this transfer function is the same in all directions; i.e., $f(\eta,\hat{n}) = f(\eta)$. In this

case, Eq. (2) simplifies, via orthogonality of the Y_{lm}s, yielding [58, 60],

$$T_{lm} = \frac{4\pi i^l}{(2\pi)^3} \int d\eta\, f(\eta) \int d^3k\, \Phi_{\vec{k}} j_l[k(\eta_0-\eta)] Y^*_{lm}(\hat{k}). \quad (3)$$

The temperature power spectrum is then easily obtained using Eq. (3), averaging over realizations of the potential perturbation, and using the identity $\langle \Phi(\vec{k})\Phi^*(\vec{k'})\rangle = (2\pi)^3\, \delta^3_D(\vec{k}-\vec{k'}) P_\Phi(k)$, where $\delta^3_D(\vec{k}-\vec{k'})$ is the Dirac delta function and $P_\Phi(k)$ the primordial-potential power spectrum, and the angle brackets denote an average over realizations of the primordial potential. We then find [59],

$$\langle T^*_{l'm'} T_{lm}\rangle = C_l^{\rm TT} \delta_{ll'} \delta_{mm'}, \quad (4)$$

where

$$C_l^{\rm TT} = \frac{2}{\pi} \int k^2\, dk\, P_\Phi(k) [T_l(k)]^2, \quad (5)$$

is the CMB temperature power spectrum, written in terms of a transfer function,

$$T_l(k) = \int d\eta\, f(\eta) j_l[k(\eta_0-\eta)]. \quad (6)$$

This transfer function is tabulated by Boltzmann codes like CAMB [61] and CMBFAST [58], and δ_{ij} is the Kronecker delta.

C. Temperature anisotropies with CIPs: Single CIP realization

In the presence of a compensated isocurvature perturbation, the baryon and dark-matter fractions vary from one point in the Universe to another, and so the transfer function $f(\eta, \hat{n})$ now obtains some direction $\hat{n}$ dependence. The CIP involves small changes,

$$\begin{aligned} \Omega_{\rm b} &\to \Omega_{\rm b}\left[1 + \Delta\left(\hat{n}\right)\right], \\ \Omega_{\rm c} &\to \Omega_{\rm c} - \Omega_{\rm b}\Delta\left(\hat{n}\right), \end{aligned} \quad (7)$$

in the cosmological parameters between different lines of sight $\hat{n}$. Here, $\Delta(\hat{n})$ is the value of the CIP in direction $\hat{n}$ at the surface of last scatter (or reionization—we will make these statements more precise below). Note that we define it so that it is the fractional perturbation in the baryon (rather than dark-matter) density associated with the CIP. From Eq. (7), the change in the total density $\delta\Omega_{\rm m} = \delta\Omega_{\rm c} + \delta\Omega_{\rm b} = 0$, and so this is indeed a compensated isocurvature perturbation.

In a general treatment of perturbed recombination/decoupling, one would follow the set of equations for the electron, dark matter, photon, and neutrino densities, velocities, and the gravitational potential at second order, as in Refs. [62–64]. In the case of CIPs, however, the CIP amplitude does not evolve for all observationally accessible scales, and we can thus model the effect of CIPs as a modulation in the cosmological parameters $\Omega_{\rm c}$ and $\Omega_{\rm b}$.

We can build some intuition for the effect of CIP perturbations on the CIP by considering a globally constant CMB perturbation Δ. We run the CAMB [61] code with a global perturbation of the form in Eq. (7) for a variety of Δ values. We evaluate the angular sound horizon l_s at the surface of last scatter as a function of Δ, using the expressions in Ref. [65]. We see in the top left panel of Fig. 1 that as the plasma is more loaded down with baryons in the presence of a CIP with a positive Δ value, the decrease in sound speed moves the CMB acoustic peaks to smaller angular scales.

CMB temperature anisotropies are suppressed on angular scales $l > l_{\rm d}$ due to diffusion damping. Using the expressions in Ref. [60] and the CAMB [61] code, we evaluate $l_d(\Delta)$ and show the results in the top right panel of Fig. 1. We see that as photons diffuse over smaller distances, as a result of higher local baryon density in the presence of a CIP with positive Δ, the transition to exponential damping of CMB anisotropies occurs at higher l.

In the bottom panel of Fig. 1 we show the visibility functions $g(z) = e^{-\tau} d\tau/dz$ for 3 different values of Δ; τ is the optical depth due to Thomson scattering. The peak of the visibility function is the redshift $z_{\rm SLS}$ at which most CMB photons last scatter. In the presence of a positive (negative) Δ CIP, decoupling occurs later (earlier) due to higher (lower) baryon density.

To calculate the effects on the CMB moments T_{lm}, we perturb the line-of-sight solutions, Eqs. (2) and (3). This approach is relatively simple and amenable to rapid computation. The results should be accurate for multipole moments $L \lesssim 870$ for the CIP, as the baryon fluctuation can be considered as roughly constant in a given direction $\hat{n}$ across the thickness of the surface of last scatter on such scales. We discuss in Section IV A below how we extrapolate these results to smaller angular scales ($L \gtrsim 870$) with a Limber approximation.

We proceed by Taylor expanding in real space,

$$\begin{aligned} f(\eta, \hat{n}) &= f^{(0)}(\eta) + \Delta(\hat{n}) \frac{df^{(0)}}{d\Delta}(\eta) \\ &+ \frac{1}{2}\Delta^2(\hat{n}) \frac{d^2 f^{(0)}}{d^2\Delta}(\eta) + \cdots, \end{aligned} \quad (8)$$

where $f^{(0)}(\eta)$ is the value of f under the null hypothesis $\Delta(\hat{n}) = 0$. We expand

$$\Delta(\hat{n}) = \sum_{LM} \Delta_{LM} Y_{LM}(\hat{n}), \quad (9)$$

in terms of spherical-harmonic coefficients Δ_{LM} for the angular variation in the CIP at the surface of last scatter. We then apply the expansion in Eq. (8) to linear order in Δ to the line-of-sight expression, Eq. (2), and integrate

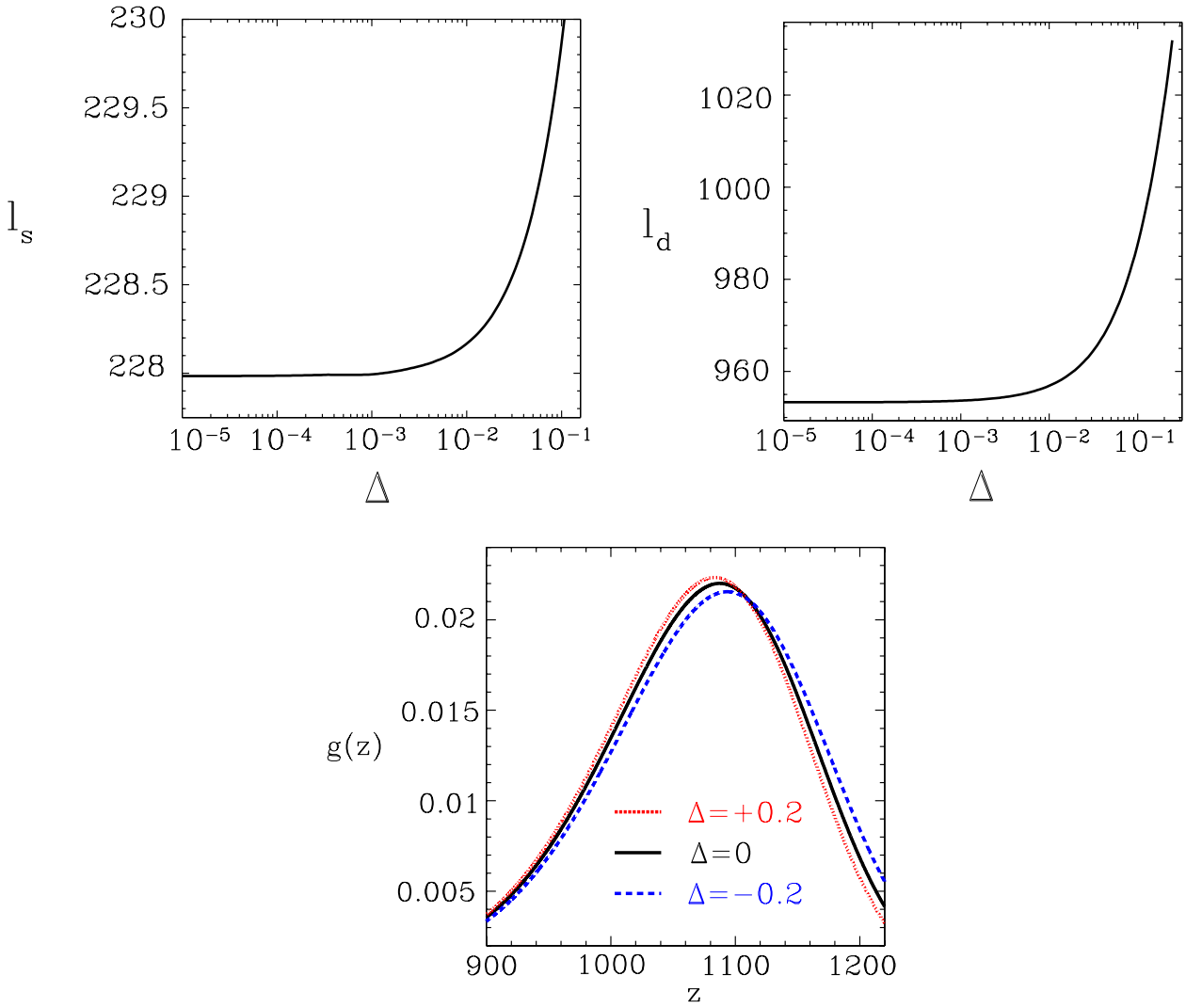

FIG. 1: Dependence of physically relevant scales and Thomson scattering visibility function $g(z)$ on amplitude of a global CIP perturbation Δ. Top left panel shows dependence of the angular sound horizon $l_{\rm s}$ on Δ. Top right panel shows dependence of the diffusion damping scale $l_{\rm d}$ on Δ. Bottom panel shows $g(z)$ evaluated for 3 different values of Δ.

over angles to obtain the first-order correction,

$$\delta T_{lm}^{(1)} = 4\pi \sum_{LM,l_1m_2} i^{l_1} \Delta_{LM} \xi^{LM}_{lml_1m_1} K^L_{ll_1} \times \int d\eta \frac{df^{(0)}}{d\Delta} \int \frac{d^3k}{(2\pi)^3} \Phi_{\vec{k}} j_l[k(\eta_0 - \eta)], \quad (10)$$

to T_{lm} in the presence of a CIP, where

$$\xi^{LM}_{lml_1m_1} \equiv \left(K^L_{ll_1}\right)^{-1} \int d\hat{n} Y^*_{lm}(\hat{n}) Y_{LM}(\hat{n}) Y_{l_1m_1}(\hat{n}) = (-1)^m \sqrt{\frac{(2L+1)(2l+1)(2l_1+1)}{4\pi}} \times \begin{pmatrix} l & L & l_1 \\ -m & M & m_1 \end{pmatrix}, \quad (11)$$

$$K^L_{ll_1} \equiv \begin{pmatrix} l & L & l_1 \\ 0 & 0 & 0 \end{pmatrix}, \quad (12)$$

and the arrays inside parentheses are Wigner-3J symbols. Throughout we use the indices L and M exclusively for the decomposition of the CIP, while lower-case indices are used for the multipole moments of the CMB observables T_{lm}, E_{lm}, and B_{lm}. Sums over m (M) are always taken over the range $-l \le m \le l$ ($-L \le M \le L$), while sums over l (L) are formally taken over $1 \le l \le \infty$ ($1 \le L \le \infty$); in practice, a maximum value $l_{\rm max}$ is used for numerical evaluation, as discussed in Sec. IV. The monopole $L = 0$ corresponds to a global shift in Ω_b and Ω_c and we absorb this term into the cosmological parameters themselves.

For a given realization of the CIP field—that is, for a given set of Δ_{LM}—the covariance between temperature moments is now

$$\langle T^*_{l'm'} T_{lm} \rangle \simeq C_l^{\rm TT,(0)} + \sum_{LM} \Delta_{LM} \xi^{LM}_{lml'm'} S^{L,\rm TT}_{ll'}, \quad (13)$$

where

$$S_{ll'}^{L,\mathrm{TT}} \equiv \left(C_{l'}^{\mathrm{T,dT}} + C_{l}^{\mathrm{T,dT}}\right) K_{ll'}^{L}, \tag{14}$$

and

$$C_l^{\mathrm{X,dX'}} \equiv \frac{2}{\pi}\int k^2\, dk\, P_\Phi(k) X_l(k) \frac{dX_l'(k)}{d\Delta}, \tag{15}$$

for $\{\mathrm{X},\mathrm{X}'\} \in \{\mathrm{T},\mathrm{E},\mathrm{B}\}$ (a generalization that will be useful below), and $C_l^{\mathrm{TT},(0)}$ is the temperature power spectrum in the absence of CIPs. Here,

$$\frac{dX_l'(k)}{d\Delta} = \int d\eta \frac{df(\eta)}{d\Delta} j_l[k(\eta_0-\eta)] \tag{16}$$

describes the change in the transfer function, Eq. (6), with Δ.

In deriving these results, we have taken an average over realizations of the primordial potential power spectrum $\Phi_{\vec{k}}$, but we have restricted our consideration to a given realization of the CIP. In Sec. V, we build the formalism to reconstruct $\Delta(\hat{n})$ from these off-diagonal temperature correlations as well their generalization to polarization.

D. Temperature anisotropies with CIPs: average over CIP realizations

We now take an ensemble average over many realizations of both the primordial potential field and the CIP field. This allows us, given a spectrum of CIPs, to calculate the effects of these CIPs on the power spectrum of CMB fluctuations measured on the entire sky.

We denote the ensemble average of a spatially varying field X over realizations of the CIP field by $\langle X\rangle_{\mathrm{b}}$. We denote the ensemble average over realizations of both the CIP field and the primordial potential by $\langle X\rangle_{\mathrm{bc}}$. From Eqs. (13)–(14), we see that $\langle T_{l'm'}^* T_{lm}\rangle_{\mathrm{bc}} \propto \langle \Delta_{LM}\rangle_{\mathrm{b}}$. For an isotropic random field, $\langle \Delta_{LM}\rangle_{\mathrm{b}} = 0$, so we must thus go to second order in $\Delta(\hat{n})$ to compute the effects of CIPs on the CMB power spectrum. We thus obtain, to second order in Δ, the temperature power spectrum,

$$\begin{aligned} C_l^{\mathrm{TT},(2)} \equiv \left\langle |T_{lm}|^2\right\rangle_{\mathrm{bc}} \simeq C_l^{\mathrm{TT},(0)} + \left\langle \left|\delta T_{lm}^{(1)}\right|^2\right\rangle_{\mathrm{bc}} \\ + \left\langle T_{lm}^{(0)*}\delta T_{lm}^{(2)}\right\rangle_{\mathrm{bc}} + \left\langle \delta T_{lm}^{(2)*} T_{lm}^{(0)}\right\rangle_{\mathrm{bc}}, \end{aligned} \tag{17}$$

where $T_{lm}^{(0)}$ is the unperturbed moment in Eq. (3), $\delta T_{lm}^{(1)}$ is given by Eq. (10), and $C_l^{\mathrm{TT},(0)}$ is the unperturbed power spectrum given by Eq. (5). The $^{(2)}$ superscript denotes the term arising when expanding T_{lm} to order $\Delta^2(\hat{n})$. We evaluate this term using the second-derivative term $d^2 f^{(0)}/d\Delta^2$ in Eq. (C2). We take an expectation value over CIPs and primordial-potential realizations. We then use Eqs. (2), Eq. (11), Eq. (17), identities of Wigner-3J symbols [66], and Appendix C to obtain

$$\begin{aligned} C_l^{\mathrm{TT},(2)} &= C_l^{\mathrm{TT},(0)} + \delta C_l^{\mathrm{TT},(1)} + \delta C_l^{\mathrm{TT},(2)} \\ \delta C_l^{\mathrm{TT},(1)} &\equiv \sum_{L,l_1} C_L^\Delta C_{l_1}^{\mathrm{dT,dT}} \left(K_{ll_1}^L\right)^2 G_{Ll_1}, \\ G_{Ll_1} &\equiv \left[\frac{(2L+1)(2l_1+1)}{4\pi}\right], \end{aligned} \tag{18}$$

$$\delta C_l^{(2)} \equiv \Delta_{\mathrm{bc}}^2 C_l^{\mathrm{T,d^2T}}. \tag{19}$$

The CIP power spectrum C_L^Δ and total variance Δ_{bc}^2 obey

$$\left\langle |\Delta_{LM}|^2\right\rangle_b \equiv C_L^\Delta, \tag{20}$$

$$\Delta_{\mathrm{bc}}^2 = \sum_L \left(\frac{2L+1}{4\pi}\right) C_L^\Delta, \tag{21}$$

while the CMB derivative power spectra are given by

$$C_l^{\mathrm{dX,dX'}} = \frac{2}{\pi}\int k^2\, dk\, P_\Phi(k) \frac{dX_l(k)}{d\Delta}\frac{dX_l'(k)}{d\Delta}, \tag{22}$$

$$C_l^{\mathrm{X,d^2X'}} = \frac{2}{\pi}\int k^2\, dk\, P_\Phi(k) X_l(k) \frac{d^2X_l'(k)}{d\Delta^2}, \tag{23}$$

where $d^2X_l/d^2\Delta$ are defined analogously to the first-derivative transfer function in Eq. (16). Appendix B details the calculation of the derivative power spectra.

III. PERTURBED LINE-OF-SIGHT FORMALISM: POLARIZATION

We now generalize the analysis above to the CMB polarization. In addition to inducing off-diagonal correlations in the polarization spherical-harmonic coefficients, CIPs will induce B modes. We begin by reviewing the LOS solution for polarization under the null hypothesis of no CIPs. We then compute the effects of CIPs, both for a single realization of the CIPs, and then for an average over realizations of a spectrum of CIPs.

A. Polarization anisotropies with homogeneous baryon fraction

Polarization is a spin-2 tensor field, and can be expanded as [67, 68]

$$P_{ab}(\hat{n}) = \sum_{lm}\left(E_{lm} Y_{lm,ab}^{\mathrm{E}} + B_{lm} Y_{lm,ab}^{\mathrm{B}}\right), \tag{24}$$

where $Y_{lm,ab}^{\mathrm{E}}$ and $Y_{lm,ab}^{\mathrm{B}}$ are the E and B mode ('grad' and 'curl', respectively) tensor spherical harmonics, as defined in Appendix A. The rightmost indices after the comma are tensor indices. In terms of the Stokes polarization parameters Q and U, the polarization tensor is [67, 68]

$$P_{ab}(\hat{n}) = \frac{1}{2}\begin{pmatrix} Q(\hat{n}) & -U(\hat{n})\sin\theta \\ -U(\hat{n})\sin\theta & -Q(\hat{n})\sin^2\theta \end{pmatrix}, \tag{25}$$

where θ is the polar angle of the LOS with respect to some origin.

Under the null hypothesis, the polarization pattern at the surface of last scatter is a pure E mode, with multipole moments given by

$$E_{lm} = \frac{4\pi i^l}{(2\pi)^3}\int d\eta\, f^{\rm E}(\eta)\int d^3k\Phi_{\vec{k}} j_l(x)Y^*_{lm}(\hat{k}), \quad (26)$$

where $x \equiv k(\eta_0-\eta)$, and $f^E(\eta)$ is the E-mode transfer function obtainable numerically from Boltzmann codes. The polarization covariance and TE covariance are derived analogously to the results for temperature, yielding [58]

$$\begin{aligned}\langle E^*_{l'm'}E_{lm}\rangle &= C_l^{\rm EE}\delta_{ll'}\delta_{mm'},\\ C_l^{\rm EE} &= \frac{2}{\pi}\int k^2dkP_\Phi(k)[E_l(k)]^2,\\ E_l(k) &= \int d\eta f^{\rm E}(\eta)j_l[k(\eta_0-\eta)],\end{aligned} \quad (27)$$

and [58]

$$\begin{aligned}\langle E^*_{l'm'}T_{lm}\rangle &= C_l^{\rm TE}\delta_{ll'}\delta_{mm'},\\ C_l^{\rm TE} &= \frac{2}{\pi}\int k^2dkP_\Phi(k)T_l(k)E_l(k).\end{aligned} \quad (28)$$

B. Polarization anisotropies with CIPs: single CIP realization

We now generalize the analysis to include the effects of CIPs. In the presence of a CIP field $\Delta(\hat{n})$, the real-space polarization tensor may be Taylor expanded as

$$\begin{aligned}P_{ab}(\hat{n}) &= P^{(0)}_{ab}(\hat{n}) + \frac{dP^{(0)}_{ab}}{d\Delta}(\hat{n})\Delta(\hat{n})\\ &+ \frac{1}{2}\frac{d^2P^{(0)}_{ab}}{d\Delta^2}(\hat{n})\,\Delta^2(\hat{n}) + \cdots .\end{aligned} \quad (29)$$

Just as in the case of temperature, when considering a single realization, we need only consider the first-order terms in Eq. (29). We then utilize Eqs. (24), (26), and the first-derivative piece of the usual expansion for $\Delta(\hat{n})$ [see Eq. (8)] to obtain an expansion for the polarization tensor P_{ab} in the presence of CIPs:

$$\begin{aligned}P_{ab}(\hat{n}) &= P_{ab}|^{\Delta=0} + \delta P_{ab}|^1 + \delta P_{ab}|^2 + \cdots, \quad (30)\\ \delta P^{(1)}_{ab} &\equiv \sum_{l_1m_1}\frac{dE_{l_1m_1}}{d\Delta}Y^E_{l_1m_1,ab}(\hat{n})\Delta(\hat{n})\\ &= \sum_{l_1m_1}^{LM}\frac{dE_{l_1m_1}}{d\Delta}Y^E_{l_1m_1ab}(\hat{n})\Delta_{LM}Y_{LM}(\hat{n}). \quad (31)\end{aligned}$$

We may now pick off the induced E and B-mode multipole moments $\delta E^{(1)}_{lm}$ and $\delta B^{(1)}_{lm}$ at order Δ, using the appropriate integral over a tensor spherical harmonic:

$$\delta E^{(1)}_{lm} = \int d\hat{n}\, Y^{\rm E,*}_{lm,ab}(\hat{n})\,\delta P^{(1)}_{ab}, \quad (32)$$

$$B_{lm} = \delta B^{(1)}_{lm} = \int d\hat{n}\, Y^{\rm B,*}_{lm,ab}(\hat{n})\,\delta P^{(1)}_{ab}. \quad (33)$$

We evaluate Eqs. (32)–(33), calling on Eqs. (A10), (A11), and (A12), yielding

$$\delta E^{(1)}_{lm} = \sum_{LM,l_1m_1}^{L+l_1+l\ \text{even}}\xi^{LM}_{lm,l_1m_1}H^L_{ll_1}\Delta_{LM}\frac{dE_{l_1m_1}}{d\Delta}, \quad (34)$$

$$\delta B^{(1)}_{lm} = \sum_{LM,l_1m_1}^{L+l_1+l\ \text{odd}}(-i)\,\xi^{LM}_{lm,l_1m_1}H^L_{ll_1}\Delta_{LM}\frac{dE_{l_1m_1}}{d\Delta}, \quad (35)$$

where

$$H^L_{ll_1} \equiv \begin{pmatrix} l & L & l_1\\ 2 & 0 & -2\end{pmatrix}. \quad (36)$$

We now evaluate the induced covariances between different temperature/polarization moments. At first order in $\Delta(\hat{n})$, $\langle B^*_{l'm'}B_{lm}\rangle \propto \langle B^{*(0)}_{l'm'}\delta B^{(1)}_{lm}\rangle = 0$. The remaining covariances are

$$\begin{aligned}\langle E^*_{l'm'}E_{lm}\rangle &= C_l^{\rm EE}\delta_{ll'}\delta_{mm'}\\ &+ \sum_{LM}^{L+l+l'\ \text{even}}\Delta_{LM}\xi^{LM}_{lm,l'm'}S^{L,\rm EE}_{ll'},\\ S^{L,\rm EE}_{ll'} &\equiv \left(C_l^{\rm E,dE}+C_{l'}^{\rm E,dE}\right)H^L_{ll'}, \quad (37)\\ \langle E^*_{l'm'}B_{lm}\rangle &= \sum_{LM}^{L+l+l'\ \text{odd}}\Delta_{LM}\xi^{LM}_{lm,l'm'}S^{L,\rm EB}_{ll'},\\ S^{L,\rm EB}_{ll'} &\equiv -iC_{l'}^{\rm E,dE}H^L_{ll'}, \quad (38)\\ \langle T^*_{l'm'}B_{lm}\rangle &= \sum_{LM}^{L+l+l'\ \text{odd}}\Delta_{LM}\xi^{LM}_{lm,l'm'}S^{L,\rm TB}_{ll'},\\ S^{L,\rm TB}_{ll'} &\equiv -iC_{l'}^{\rm T,dE}H^L_{ll'}, \quad (39)\\ \langle T^*_{l'm'}E_{lm}\rangle &= C_l^{\rm TE}\delta_{ll'}\delta_{mm'}\\ &+ \sum_{LM}^{L+l+l'\ \text{even}}\Delta_{LM}\xi^{LM}_{lm,l'm'}S^{L,\rm TE}_{ll'},\\ S^{L,\rm TE}_{ll'} &\equiv \left(C_{l'}^{\rm T,dE}H^L_{ll'}+C_l^{\rm E,dT}K^L_{ll'}\right). \quad (40)\end{aligned}$$

C. Polarization anisotropies with CIPs: average over CIP realizations

We now extend the ensemble average to multiple realizations of the CIP field. We do this in order to compare the polarization power spectrum induced by CIPs at the surface of last scatter with that induced at reionization. For temperature, the average over realizations of both the

CIP and primordial potential perturbations is given by Eq. (17). Extending this average to $X, X' \in \{T, E, B\}$, we obtain the XX′ power spectra, averaged over the entire sky, to second order in Δ:

$$\begin{aligned} C_l^{\mathrm{XX}',(2)} &\equiv \left\langle X_{lm} X'^{*}_{lm} \right\rangle_{\mathrm{bc}} \\ &\simeq C_l^{\mathrm{XX}',(0)} + \left\langle \delta X^{(1)}_{lm} \delta X'^{(1)}_{lm} \right\rangle_{\mathrm{bc}} \\ &+ \left\langle X^{(0)*}_{lm} \delta X'^{(2)}_{lm} \right\rangle_{\mathrm{bc}} + \left\langle \delta X^{(2)*}_{lm} X'^{(0)}_{lm} \right\rangle_{\mathrm{bc}}. \end{aligned} \quad (41)$$

We evaluate Eq. (41) with Eqs. (A12)–(A13) and Wigner-3J relations to simplify the resulting integrals and sums. Superscript indices $^{(1)}$ and $^{(2)}$ indicate the order of the derivative $d^n f^{(0)}/d\Delta^n$ used to derive the indicated term, as in Sec. II D. The resulting non-zero power spectra are

$$\begin{aligned} C_l^{\mathrm{TE}} &\simeq C_l^{\mathrm{TE},(0)} + \delta C_l^{\mathrm{TE},(1)} + \delta C_l^{\mathrm{TE},(2)} \quad (42) \\ \delta C_l^{\mathrm{TE},(1)} &\equiv \sum_{L,l_1}^{L+l_1+l \text{ even}} C_L^{\Delta} C_{l_1}^{\mathrm{dT,dE}} G_{Ll_1} H^L_{ll_1} K^L_{ll_1} \\ \delta C_l^{\mathrm{TE},(2)} &\equiv \frac{\Delta^2_{\mathrm{bc}}}{2} \left(C_l^{\mathrm{T,d^2E}} + C_l^{\mathrm{E,d^2T}} \right), \end{aligned}$$

$$\begin{aligned} C_l^{\mathrm{EE}} &\simeq C_l^{\mathrm{EE},(0)} + \delta C_l^{\mathrm{EE},(1)} + \delta C_l^{\mathrm{EE},(2)}, \quad (43) \\ \delta C_l^{\mathrm{EE},(1)} &\equiv \sum_{L,l_1}^{L+l_1+l \text{ even}} C_L^{\Delta} C_{l_1}^{\mathrm{dE,dE}} G_{Ll_1} \left(H^L_{ll_1} \right)^2, \\ \delta C_l^{\mathrm{EE},(2)} &= \Delta^2_{\mathrm{bc}} C_l^{\mathrm{E,d^2E}}, \end{aligned}$$

and

$$C_l^{\mathrm{BB}} \simeq \sum_{L,l_1}^{L+l_1+l \text{ odd}} C_L^{\Delta} C_{l_1}^{\mathrm{dE,dE}} G_{Ll_1} \left(H^L_{ll_1} \right)^2. \quad (44)$$

The CIP field $\Delta(\hat{n})$ is a scalar, and cannot statistically change the parity of polarization perturbations. This requires that C_l^{TB} and C_l^{EB} vanish when averaging over CIP realizations. Algebraically, this is enforced by the vanishing of the relevant Wigner-3J symbols, as occurs with optical-depth fluctuations at reionization [44, 69] and with gravitational-potential perturbations in weak lensing [70, 71]. Indeed, the geometric (Wigner-3J) symbols obtained are the same as for those effects. CIPs give rise to different ll' dependences for the functions $S^{L,\mathrm{XX}'}_{ll'}$, however, through the dependence on the derivative power spectra $C_l^{\mathrm{XX}'}$, allowing them to be disentangled observationally from gravitational potential fluctuations along the line of sight or optical-depth fluctuations at reionization.

IV. NUMERICAL RESULTS FOR B MODE POWER SPECTRA

We now apply the formulas derived in Secs. II D and III C to compute the power spectra for B modes induced by CIPs at decoupling. We first discuss the form of the angular CIP power spectrum C_L^{Δ}. We then present numerical results for B modes induced at decoupling. For comparison, we then reproduce the calculations of Ref. [35] of the B modes induced at reionization.

A. Power spectrum of compensated perturbations

1. Three-dimensional CIP power spectrum

To proceed further we must make an *ansatz* for the spectrum of CIPs. Motivated by the curvaton model (which produces a nearly scale invariant spectrum of CIPs) [34, 36, 47], we assume a scale-invariant spectrum, for the three-dimensional CIP field $\Delta(\mathbf{x})$; that is,

$$\begin{aligned} \left\langle \tilde{\Delta}^*(\mathbf{k}') \tilde{\Delta}(\mathbf{k}) \right\rangle &= (2\pi)^3 \delta_D^3 \left(\mathbf{k} - \mathbf{k}' \right) P_{\Delta}(k) \\ P_{\Delta}(k) &= A k^{-3}, \end{aligned} \quad (45)$$

where $\tilde{\Delta}(\mathbf{k})$ is the Fourier transform of $\Delta(\mathbf{x})$, and A is a dimensionless CIP amplitude.

As discussed in the Introduction, the strongest constraint to A comes from cluster baryon fractions. This constraint tells us that the variance,

$$\Delta^2_{\mathrm{cl}} = \frac{1}{2\pi^2} \int k^2 \, dk \, \left[3 j_1(kR)/(kR) \right]^2 P_{\Delta}(k), \quad (46)$$

in the baryon–to–dark-matter ratio on $R \sim 10$ Mpc scales is $\Delta_{\mathrm{cl}} \lesssim 0.08$. The integral has a formal logarithmic divergence at low k which is cut off, however, by the volume occupied by the clusters surveyed. Taking this to be the horizon, $k_{\mathrm{min}} \simeq (10 \text{ Gpc})^{-1}$, we find $A \lesssim 0.017$.

2. Angular CIP power spectrum

When the three-dimensional field is projected onto a narrow spherical surface, the resulting angular power spectrum for Δ will be $C_L^{\Delta} \simeq A/(\pi L^2)$ for mulipole moments $L \lesssim (\eta_0 - \eta_{\mathrm{ls}})/\sigma_\eta \simeq 870$, where η_{ls} and η_0 are the conformal time at last scatter and today, respectively, and σ_η is the rms conformal-time width of the last-scattering surface. At smaller angular scales (larger L), the angular variation in Δ is suppressed by the finite width [72] of the scattering surface. Using the Limber approximation, the angular power spectrum for Δ can be approximated by $C_L^{\Delta} \simeq A(\eta_0 - \eta_{\mathrm{ls}})/(2\sqrt{\pi} L^3 \sigma_\eta)$ for $L \gtrsim 870$. The exact analytic expression we use is obtained from the Limber approximation, approximating the visibility function as a Gaussian. It is

$$C_L^{\Delta} = \frac{A}{2\sqrt{\pi} L^2} U \left[\frac{1}{2}, 0, \left(\frac{L \sigma_\eta}{\eta_0 - \eta_{\mathrm{sls}}} \right)^2 \right], \quad (47)$$

where $U(a, b, x)$ is a confluent hypergeometric function. We use $\eta_0 - \eta_{\mathrm{ls}} = 14100$ Mpc and $\sigma_\eta = 16.2$ Mpc for decoupling. We use $\eta_0 - \eta_{\mathrm{ls}} = 9760$ Mpc and $\sigma_\eta = 448$ Mpc

for reionization. These values are obtained by directly fitting to the visibility function output by the CAMB code [61]. Of course Eq. (47) is an approximation, and the precise shape of the transition from $C_L^\Delta \propto 1/L^2 \to C_L^\Delta \propto 1/L^3$ near $L \sim 870$ depends on the interference of Fourier modes of Δ with those of Φ, averaged over the SLS. This issue warrants future study, but the asymptotic behavior at low and high L is correct (as shown for an analogous computation in Ref. [73]). Moreover, as we shall see in Sec. VI, most signal-to-noise in CIP reconstruction comes either from $L \lesssim 100$ or $L \gtrsim 2000$, and so the main conclusions of this work should not be affected.

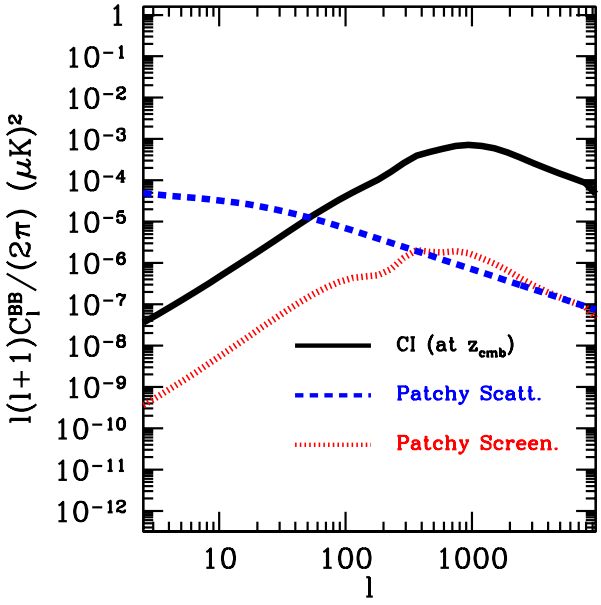

FIG. 2: CMB B-mode polarization power spectra induced by CIP perturbations at decoupling (black solid line), compared with the effects of CIPs at reionization, for which two contributions are shown: patchy screening (red dotted line), and patchy scattering (blue short-dashed line). The amplitude for the CIP power spectrum is that which saturates the $\Delta_{\rm cl} \lesssim 0.08$ bound from clusters [35].

B. Numerical result for B modes from CIPs at decoupling

Using the Limber approximation with values $\eta_0 - \eta_{\rm ls} = 14100$ Mpc and $\sigma_\eta = 16.2$ Mpc appropriate for decoupling, Eqs. (42)–(44) can be used to obtain predictions for the B modes induced by CIPs at decoupling. The results are shown in Fig. 2 for $A = 0.017$, the largest CIP amplitude consistent with the galaxy-cluster constraint. Appendix B details the calculation of the requisite derivative power spectra. We use a maximum l value of $l_{\rm max} = 10000$.

C. Reionization

In Ref. [35] it was noted that spatial inhomogeneities in the baryon density give rise to angular variations in the optical depth τ for re-scattering of CMB photons at reionization. It was also noted that these inhomogeneities would give rise to B modes primarily at large angular scales by patchy re-scattering of CMB photons and at smaller angular scales through patchy screening of the primary CMB polarization from the decoupling epoch. These calculations build upon calculations in Refs. [44, 69, 74–76] where optical-depth fluctuations were postulated to arise from inhomogneities in the free-electron fraction due to inhomogeneous reionization.

In our notation, the contribution of patchy screening is [44, 69]

$$C_l^{\rm TT} = \tau^2 e^{-2\tau} \sum_{L,l_1} C_L^\Delta C_{l_1}^{\rm TT,rec} \left(K_{ll_1}^L\right)^2 G_{Ll_1} \tag{48}$$

$$\delta C_l^{\rm TE} = \tau^2 e^{-2\tau} \sum_{L,l_1}^{L+l_1+l\ \rm even} C_L^\Delta C_{l_1}^{\rm TE,rec} K_{ll_1}^L H_{ll_1}^L G_{Ll_1}, \tag{49}$$

$$\delta C_l^{\rm EE} = \tau^2 e^{-2\tau} \sum_{L,l_1}^{L+l_1+l\ \rm even} C_L^\Delta C_{l_1}^{\rm EE,rec} \left(H_{ll_1}^L\right)^2 G_{Ll_1}, \tag{50}$$

$$\delta C_l^{\rm BB} = \tau^2 e^{-2\tau} \sum_{L,l_1}^{L+l_1+l\ \rm odd} C_L^\Delta C_{l_1}^{\rm EE,rec} \left(H_{ll_1}^L\right)^2 G_{Ll_1}, \tag{51}$$

where $\tau = 0.086$ is the mean optical depth, and C_L^Δ is here the angular CIP power spectrum *for reionization*; i.e., obtained with $\eta_0 - \eta_{\rm ls} = 9760$ Mpc and $\sigma_\eta = 448$ Mpc. These values are obtained by fitting a Gaussian visibility function to the reionization model of Ref. [77].

The contributions of patchy scattering are

$$\delta C_l^{\rm BB} = \delta C_l^{\rm EE} = \frac{3\tau^2}{100} C_l^\Delta Q_{\rm rms}^2 e^{-2\tau}, \tag{52}$$

where $Q_{\rm rms} \simeq 17.9\,\mu$K is the rms temperature quadrupole at reionization.

Fig. 2 shows the B modes induced by patchy scattering and screening at reionization again using $A = 0.017$. We see that at all but the largest scales, the decoupling-induced B modes are larger (by up to ~ 3 orders of magnitude) than those induced at reionization.

We thus conclude that the effects of CIPs on CMB fluctuations would be much larger than found in Ref. [35], particularly at the small scales most important for detection and reconstruction (to be discussed below) of CIPs from the CMB. We thus now move on to show how spatial fluctuations in the baryon–to–dark-matter ratio can be measured with CMB maps.

TABLE I: The 'response functions' $S_{ll'}^{L,\mathrm{XX}'}$ of CMB fluctuations to CIPs, defined in Eq. (13) and Eqs. (37)–(40), for the various correlation functions.

XX′	$S_{ll'}^{L,\mathrm{XX}'}$
TT	$\left(C_{l'}^{\mathrm{T,dT}}+C_{l}^{\mathrm{T,dT}}\right)K_{ll'}^{L}$
EE	$\left(C_{l}^{\mathrm{E,dE}}+C_{l'}^{\mathrm{E,dE}}\right)H_{ll'}^{L}$
EB	$-iC_{l'}^{\mathrm{E,dE}}H_{ll'}^{L}$
TB	$-iC_{l'}^{\mathrm{T,dE}}H_{ll'}^{L}$
TE	$\left(C_{l'}^{\mathrm{T,dE}}H_{ll'}^{L}+C_{l}^{\mathrm{E,dT}}K_{ll'}^{L}\right)$

V. MEASUREMENT OF CIPS WITH THE CMB

In this Section, we show how the CIP field $\Delta(\hat{n})$ can be measured with higher-order CMB correlations, building upon analogous prior work on measurement of cosmic-shear fields [70, 71, 78–81], departures from statistical isotropy [82–84], and cosmic birefringence [85–88]. Having concluded that the decoupling signal is much bigger than that from reionization, we consider detection/measurement of CIPs at the surface of last scatter.

In Sec. V A, we construct a minimum-variance quadratic estimator $\widehat{\Delta}_{LM}$ for the multipole moments of the CIP field. In Sec. V B, we explicitly calculate the noise covariance (due both to cosmic variance and experimental noise) needed to evaluate the errors and optimal weights of Sec. V A. Finally, in Sec. V C, we use the results of the preceding sections to derive an expression for the signal-to-noise ratio (SNR) with which a CMB experiment can detect CIPs.

A. Minimum-variance estimators for Δ_{LM}

The total correlation between multipole moments (including the contribution induced by a given realization of CIPs) takes the form [see Eq. (13) and Eqs. (37)–(40)],

$$\left\langle X_{l'm'}^{'*}X_{lm}\right\rangle = C_{l}^{\mathrm{XX}'}\delta_{ll'}\delta_{mm'}+\sum_{LM}D_{ll'}^{LM,\mathrm{XX}'}\xi_{lm,l'm'}^{LM}, \tag{53}$$

where

$$D_{ll'}^{LM,\mathrm{XX}'}\equiv\Delta_{LM}S_{ll'}^{L,\mathrm{XX}'}.$$

As before, $\mathrm{X},\mathrm{X}'\in\{\mathrm{T},\mathrm{E},\mathrm{B}\}$. As discussed in Secs. II and III, the functions $S_{ll'}^{L,\mathrm{XX}'}$ map Δ_{LM} to observed off-diagonal CMB anisotropies. The $S_{ll'}^{LM,\mathrm{XX}'}$ are assembled in Table I.

The spherical-harmonic coefficients X_{lm}^{map} obtained by a given CMB experiment are related to the true coefficients X_{lm} by $X_{lm}^{\mathrm{map}}=W_lX_{lm}$, where $W_l=e^{-l(l+1)\sigma_b^2/2}$ is the window function, and $\sigma_b=\theta_{\mathrm{fwhm}}/\sqrt{8\ln 2}\simeq 0.00741\,(\theta_{\mathrm{fwhm}}/1^\circ)$ is related to the beam's full width at half maximum (FWHM) θ_{fwhm}. The observed two-point correlations are then

$$\left\langle X_{l'm'}^{\prime,\mathrm{map}*}X_{lm}^{\mathrm{map}}\right\rangle = C_{l}^{\mathrm{XX}'}W_l^2\delta_{ll'}\delta_{mm'}+\sum_{LM}D_{ll'}^{LM,\mathrm{XX}',\mathrm{map}}\xi_{lm,l'm'}^{LM}, \tag{54}$$

$$D_{ll'}^{LM,\mathrm{XX}',\mathrm{map}}=D_{ll'}^{LM,\mathrm{XX}'}W_lW_{l'}. \tag{55}$$

Following Refs. [44, 69, 84–86, 88], the minimum-variance quadratic estimator for the rotational invariant $D_{ll',\mathrm{map}}^{LM,\mathrm{XX}'}$ is

$$\widehat{D}_{ll'}^{LM,\mathrm{XX}',\mathrm{map}}=(G_{ll'})^{-1}\sum_{mm'}X_{lm}^{\mathrm{map}}X_{l'm'}^{\prime,\mathrm{map}*}\xi_{lm,l'm'}^{LM}. \tag{56}$$

To extract Δ_{LM}, CMB temperature and polarization maps must be used to reconstruct $\widehat{D}_{ll'}^{LM,\mathrm{XX}',\mathrm{map}}$ by applying Eq. (56). Then, through the estimator $\widehat{\Delta}_{LM}^{ll',\mathrm{XX}'}\equiv\widehat{D}_{ll'}^{LM,\mathrm{XX}',\mathrm{map}}/\left(W_lW_{l'}S_{ll'}^{LM,\mathrm{XX}'}\right)$, we obtain many measurements of Δ_{LM}. These measurements are generally correlated (even for fixed l,l'), so we must take care to construct an optimal estimator $\widehat{\Delta}_{LM}$ for CIPs when using the full set of available maps for a given experiment. Generalizing the estimator and error formulae in Refs. [84, 86] to our case of interest, we obtain the optimal estimator $\widehat{\Delta}_{LM}$ and its rms error σ_{Δ_L}, taking into account all possible correlations between X and X′:

$$\widehat{\Delta}_{LM}=\sigma_{\Delta_{LM}}^2\sum_{l'\geq l}G_{ll'}\sum_{\mathrm{AA}'}\mathcal{Z}_{ll'}^{LM,\mathrm{A}'}\widehat{D}_{ll'}^{LM,\mathrm{A},\mathrm{map}}\left[\mathcal{C}_{ll'}^{-1}\right]_{\mathrm{AA}'},$$

$$\sigma_{\Delta_{LM}}^{-2}=\sum_{l'\geq l}G_{ll'}\sum_{\mathrm{AA}'}\mathcal{Z}_{ll'}^{LM,\mathrm{A}'}\mathcal{Z}_{ll'}^{LM,\mathrm{A}}\left[\mathcal{C}_{ll'}^{-1}\right]_{\mathrm{AA}'}, \tag{57}$$

where $\{A,A'\}\in\{\mathrm{EB},\mathrm{BE},\mathrm{TB},\mathrm{BT},\mathrm{TT},\mathrm{EE},\mathrm{TE},\mathrm{ET}\}$ when $l\neq l$, $\{A,A'\}\in\{\mathrm{EB},\mathrm{TB},\mathrm{TT},\mathrm{EE},\mathrm{TE}\}$ when $l=l'$, and

$$\mathcal{Z}_{ll'}^{LM,\mathrm{A}}\equiv S_{ll'}^{LM,\mathrm{A}}W_lW_{l'}. \tag{58}$$

The inequality $l'\geq l$ is imposed so that we do not double count correlations. Sums are subject to the additional restriction that for $\{A,A'\}\in(\mathrm{TE},\mathrm{ET},\mathrm{EE},\mathrm{TT})$, $l+l'+L$ is even, while for $\{A,A'\}\in(\mathrm{BE},\mathrm{EB},\mathrm{BT},\mathrm{TB})$, $l+l'+L$ is odd. The appropriately normalized covariance matrix for $\widehat{D}_{ll'}^{LM,\mathrm{AA}',\mathrm{map}}$ is

$$\mathcal{C}_{ll'}^{\mathrm{AA}'}\equiv G_{ll'}\left(\left\langle\widehat{D}_{ll'}^{LM,\mathrm{A},\mathrm{map}}\widehat{D}_{ll'}^{LM,\mathrm{A}',\mathrm{map}*}\right\rangle-\left\langle\widehat{D}_{ll'}^{LM,\mathrm{A},\mathrm{map}}\right\rangle\left\langle\widehat{D}_{ll'}^{LM,\mathrm{A}',\mathrm{map}*}\right\rangle\right). \tag{59}$$

We now proceed to compute the covariance matrix $\mathcal{C}_{ll'}^{\mathrm{AA}'}$.

B. Off-diagonal covariances

To numerically evaluate Eq. (59), we must have a model for the statistics of the observed map covariances, *including* noise. We assume the noise in each pixel is statistically independent, Gaussian, and uncorrelated with the signal, and we assume no coupling between the noises in {T, E, B}. In this case, the noise power spectra are [89]

$$C_l^{\rm BB,noise} = C_l^{\rm EE,noise} = 2C_l^{\rm TT,noise} = 8\pi \frac{f_{\rm survey}({\rm NET})^2}{t_{\rm obs}}, \quad (60)$$

where NET is the (effective) noise-equivalent temperature for the experiment, $t_{\rm obs}$ the duration of the experiment, and $f_{\rm survey}$ is the fraction of sky surveyed. The cross spectra $C_l^{\rm XX',noise} = 0$ if X $\neq$ X′. The power spectra for the map are

$$C_l^{XX',\ {\rm map}} \equiv C_l^{XX'} |W_l|^2 + C_l^{XX',\ {\rm noise}}. \quad (61)$$

It is useful to explicitly evaluate Eq. (59) using Eq. (56). Since all fields involved are Gaussian, all the four-point functions that arise may be evaluated using Wick's theorem. Wigner-3J identities may then be fruitfully applied to obtain all the elements of $\mathcal{C}_{ll'}^{\rm AA'}$ expressed in terms of $C_l^{\rm XX',map}$. If $l = l'$, then $\mathcal{C}_{ll}$ is a 5×5 diagonal matrix, with rows/columns in the order TT, EE, TE, BE, BT and entries

$$\mathcal{C}_{ll} = \begin{pmatrix} \mathcal{F}_{ll} & \mathbf{0} \\ \mathbf{0}^* & \mathcal{G}_{ll} \end{pmatrix}, \quad \mathcal{F}_{ll} = 2 \begin{pmatrix} \left(C_l^{\rm TT,map}\right)^2 & \left(C_l^{\rm TE,map}\right)^2 & C_l^{\rm TT,map} C_l^{\rm TE,map} \\ \left(C_l^{\rm TE,map}\right)^2 & \left(C_l^{\rm EE,map}\right)^2 & C_l^{\rm EE,map} C_l^{\rm TE,map} \\ C_l^{\rm TT,map} C_l^{\rm TE,map} & C_l^{\rm EE,map} C_l^{\rm TE,map} & \left[\left(C_l^{\rm TE,map}\right)^2 + C_l^{\rm TT,map} C_l^{\rm EE,map}\right]/2 \end{pmatrix}, \quad (62)$$

$$\mathcal{G}_{ll} = \begin{pmatrix} C_l^{\rm EE,map} C_l^{\rm BB,map} & C_l^{\rm BB,map} C_l^{\rm TE,map} \\ C_l^{\rm BB,map} C_l^{\rm TE,map} & C_l^{\rm BB,map} C_l^{\rm TT,map} \end{pmatrix}. \quad (63)$$

If $l \neq l'$, $\mathcal{C}_{ll'}$ is an 8×8 block-diagonal matrix, with rows/columns in the order TT, EE, TE, ET, BE, EB, BT, TB and entries

$$\mathcal{C}_{ll'} = \begin{pmatrix} \mathcal{N}_{ll'} & \mathbf{0} \\ \mathbf{0} & \mathcal{K}_{ll'} \end{pmatrix}, \quad \mathcal{N}_{ll'} = \begin{pmatrix} C_l^{\rm TT,map} C_{l'}^{\rm TT,map} & C_l^{\rm TE,map} C_{l'}^{\rm TE,map} & C_l^{\rm TT,map} C_{l'}^{\rm TE,map} & C_l^{\rm TE,map} C_{l'}^{\rm TT,map} \\ C_l^{\rm TE,map} C_{l'}^{\rm TE,map} & C_l^{\rm EE,map} C_{l'}^{\rm EE,map} & C_l^{\rm TE,map} C_{l'}^{\rm EE,map} & C_l^{\rm EE,map} C_{l'}^{\rm TE,map} \\ C_l^{\rm TT,map} C_{l'}^{\rm TE,map} & C_l^{\rm TE,map} C_{l'}^{\rm EE,map} & C_l^{\rm TT,map} C_{l'}^{\rm EE,map} & C_l^{\rm TE,map} C_{l'}^{\rm TE,map} \\ C_l^{\rm TE,map} C_{l'}^{\rm TT,map} & C_l^{\rm EE,map} C_{l'}^{\rm TE,map} & C_l^{\rm TE,map} C_{l'}^{\rm TE,map} & C_l^{\rm EE,map} C_{l'}^{\rm TT,map} \end{pmatrix}, \quad (64)$$

$$\mathcal{K}_{ll'} = \begin{pmatrix} C_l^{\rm BB,map} C_{l'}^{\rm EE} & 0 & C_l^{\rm BB,map} C_{l'}^{\rm TE,map} & 0 \\ 0 & C_l^{\rm EE,map} C_{l'}^{\rm BB,map} & 0 & C_l^{\rm TE,map} C_{l'}^{\rm BB,map} \\ C_l^{\rm BB,map} C_{l'}^{\rm TE,map} & 0 & C_l^{\rm BB,map} C_{l'}^{\rm TT,map} & 0 \\ 0 & C_l^{\rm TE,map} C_{l'}^{\rm BB,map} & 0 & C_l^{\rm TT} C_{l'}^{\rm BB,map} \end{pmatrix}.$$

In Sec. VI A, we apply the preceding formulae to estimate the noise in the reconstructed CIP field for a variety of

ongoing and upcoming experiments.

In many cases, most of the sensivity to CIPs comes from a single combination (e.g., TT or TB) of observables. It is therefore interesting to consider the constraining power of a single such combination. In the case of TB, the error is given by [see Eqs. (57)]

$$\sigma_{\Delta_L}^{-2} = \sum_{l'\geq l}^{l+l'+L \text{ odd}} G_{ll'} \frac{\left(S_{ll'}^{LM,\mathrm{TB}}\right)^2}{C_l^{\mathrm{BB,map}} C_{l'}^{\mathrm{TT,map}}} + \quad \{\mathrm{T}\leftrightarrow\mathrm{B}\}\,. \tag{65}$$

To generate the noise curves discussed in Sec. VI A, we use expressions analogous to Eq. (65) for each pair of observables. These noise values are then applied to estimate the signal-to-noise ratio (SNR) with which a given spectrum of CIPs might be detected.

C. Signal-to-noise formula

Ultimately, we wish to assess the SNR of our estimators for a given CIP power-spectrum amplitude A. Each estimator $\widehat{\Delta}_{LM}$ gives an independent estimator for A, and by adding them all with inverse-variance weighting, the total signal-to-noise with which CIPs can be detected is

$$S/N = \left[\frac{f_{\mathrm{sky}}}{2}\sum_{L>L_{\mathrm{min}}}(2L+1)\left(\frac{C_L}{\sigma^2_{\Delta_L}}\right)^2\right]^{1/2}, \tag{66}$$

where the error is evaluated using Eq. (57), f_{sky} is the fraction of sky used in the data analysis, and $L_{\mathrm{min}} \equiv f_{\mathrm{sky}}^{-1/2}$. Modes that vary on scales larger than the area of sky analyzed will have degraded signal-to-noise. A minimum value of L is thus imposed to conservatively account for fractional sky coverage. In practice, these modes would still contribute to the integrated CIP power in the area of sky analyzed. In this work, however, we impose a cut at L_{min} to avoid an over-estimate of sensitivity, all the same establishing the utility of CMB observations for probing CIPs.

VI. EXPERIMENTAL PROSPECTS

We now apply the formalism of Sec. V to assess the prospects of using CMB experiments to detect CIPs. We consider specifically the ongoing WMAP [90] and Planck [42] satellites and a possible future satellite, EPIC [46]. We also consider the following suborbital experiments: Polarbear [91], Spider [92] and ACT [93] and SPT [94] and their polarization upgrades ACTPol [43] and SPTPol [45]. Finally we consider an idealistic cosmic variance limited experiment, abbreviated CV, limited only by sky cuts to avoid galactic foreground emission. We do this to roughly quantify the the lowest CIP amplitudes that could ever be probed with the CMB.

The experimental parameters assumed for these experiments are given in Table II. For WMAP, Planck, EPIC, and the cosmic variance limited case, we assume that $f_{\mathrm{survey}} = 1$, while for Polarbear, SPT, ACT, SPTPol, and ACTPol, we assume that $f_{\mathrm{survey}} = f_{\mathrm{sky}}$. For WMAP, we assume use of the V and W bands in the analysis. For Planck, we assume that the 143 and 217 Ghz channels will be usable for CMB anisotropy measurements, and take appropriate inverse variance weighted sums of the noise in these channels. Appendix B details the calculation of the requisite derivative power spectra. We include BB correlations induced by gravitational lensing when evaluating $\mathcal{C}_{ll'}^{\mathrm{AA}'}$, using the CAMB lensing module [61].

Expt.	Channel	θ	NET	f_{sky}	t_{obs}
WMAP	V Band	21	1200	0.65	7
WMAP	W Band	13	1600	0.65	7
Polarbear	150 Ghz	4.0	36	0.015	1.0
Planck HFI	143 Ghz	7.1	62	0.65	1.2
Planck HFI	217 Ghz	5.0	91	0.65	1.2
Spider	150 Ghz	30	4.2	0.1	0.016
ACT	148 Ghz	1.4	58	0.0072	0.14
SPT	150 Ghz	1.2	91	0.0024	0.29
ACTPol	150 Ghz	1.4	6.0	0.10	0.21
SPTPol	150 Ghz	1.0	14	0.016	0.75
EPIC	150 Ghz	5.0	2.0	0.65	4.0
CV	–	–	0.0	0.65	–

TABLE II: Experimental parameters for the experiments considered in this work: beamwidth θ (in arcminutes), noise-equivalent temperature (NET) (in μK sec$^{1/2}$), and observation time t_{obs} (in years).

A. Noise curves

We compute the noise curves in the reconstruction $\widehat{\Delta}_{LM}$ for all experiments under consideration, and show the results in Figs. 3–6. We plot the noise power spectrum

$$\delta C_L = \frac{\sigma^2_{\Delta_L}}{f_{\mathrm{sky}}\sqrt{2L+1}} \tag{67}$$

as well as the signal C_L. We use the value $A = 0.017$, which saturates the galaxy cluster bound on CIPs. Experiments with larger beams, such as Polarbear and Spider, generally have higher noise levels (for reconstruction of Δ) than do others. At low L, temperature is generally the best probe of CIPs. At sufficiently high L, the BT correlation takes over as the best probe of CIPs. At very high L, all the noise curves grow very large, indicating that the fidelity of the reconstruction of the CIP breaks

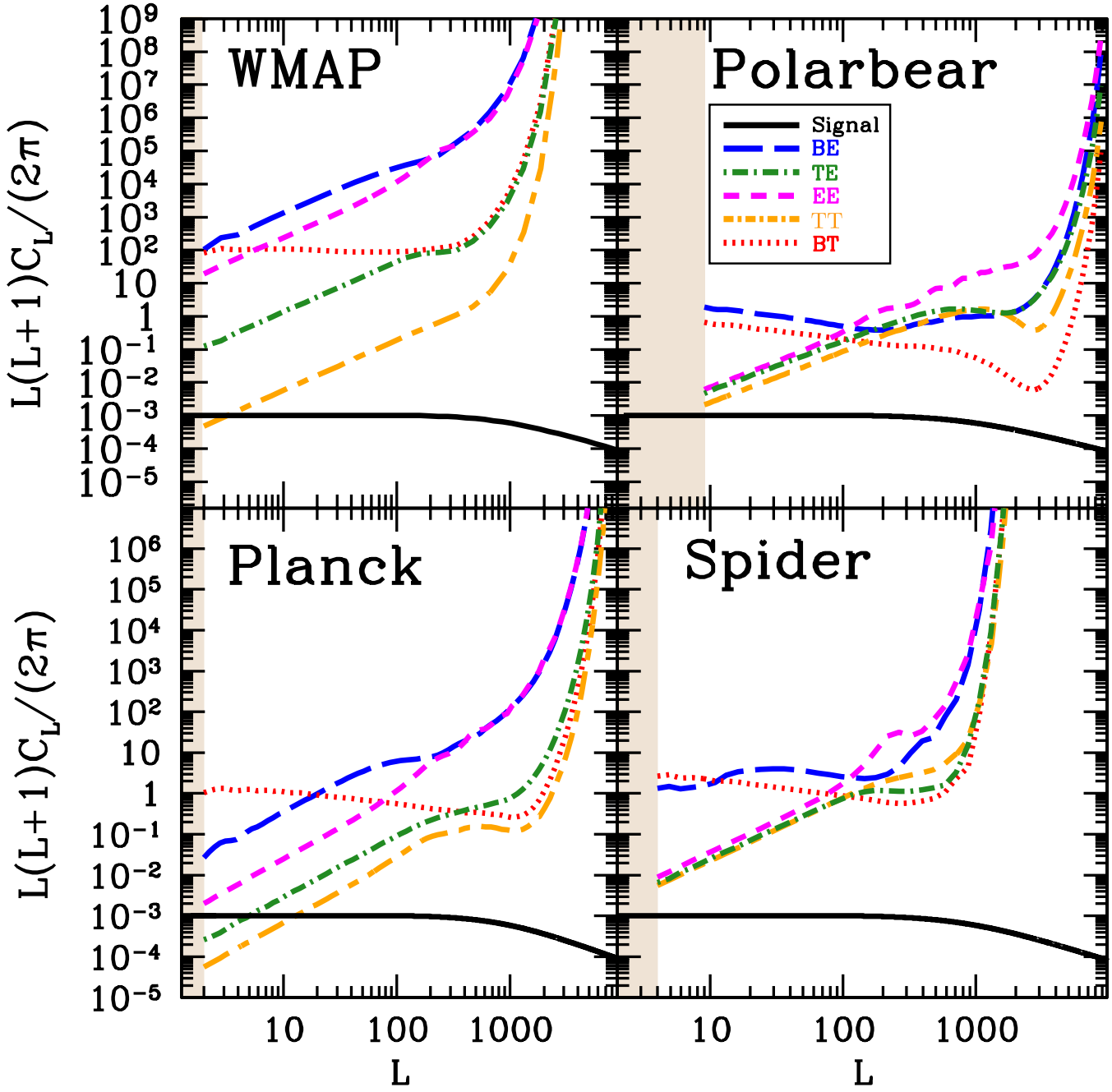

FIG. 3: Predicted noise power spectrum δC_L in the reconstructed CIP perturbation field Δ_{LM} in four different ongoing/future CMB anisotropy experiments, as a function of angular scale L. We separately plot the noise for distinct pairs of observables: TT is shown as an orange (short-dash long-dashed), TE as a green (dot-dashed) line, EE as a magenta (short-dashed) line, BE as a blue (long-dashed) line, and BT as a red (dotted) line. Also shown (black solid line) is the power spectrum C_L^{Δ} , marked signal, for a scale-invariant spectrum of CIPs with the maximum amplitude allowed by galaxy clusters. Each panel shows estimates for a different experiment, as indicated in the figure. The beige (grey) shaded region shows the range of L that is not included in our estimates, due to finite sky coverage effects, as discussed in Sec. V C.

down at small scales. This is very similar to lensing, and is expected, as fluctuations in the baryon fraction couple small to large scales. We note that $C_l^{\mathrm{XX'},\mathrm{map}}$ is computed using $\tau = 0.086$, as the observed CMB anisotropies are affected both by a screening envelope at high l, due to reionization, and by a reionization 'bump' in polarization at low l. We use CAMB's built-in *tanh* reionization model with the parameters of Ref. [77].

We then compute the total noise in the reconstruction $\widehat{\Delta}_{LM}$ for each experiment, adding the different cor-

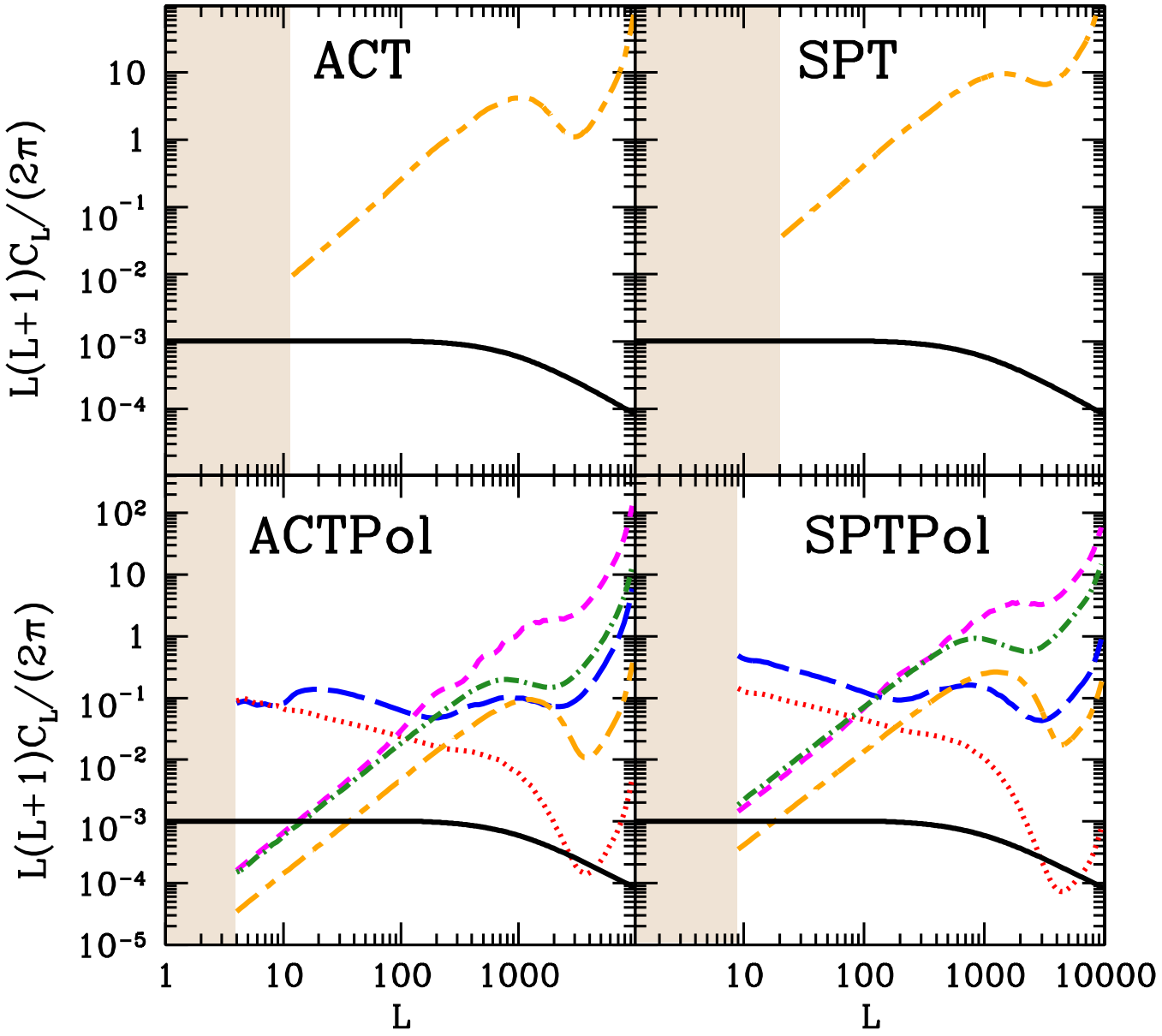

FIG. 4: Predicted noise power spectrum δC_L in the reconstructed CIP perturbation field Δ_{LM} in four different ongoing/future CMB anisotropy experiments, as a function of angular scale L. Colors (line-styles) are as in Fig. 3. We separately plot the noise for distinct pairs of observables: TT is shown as an orange (short-dash long-dashed), TE as a green (dot-dashed) line, EE as a magenta (short-dashed) line, BE as a blue (long-dashed) line, and BT as a red (dotted) line. Also shown (black solid line) is the power spectrum C_L^{Δ}, for a scale-invariant spectrum of CIPs with the maximum amplitude allowed by galaxy clusters. Each panel shows estimates for a different experiment, as indicated in the figure. The beige (grey) shaded region shows the range of L that is not included in our estimates, due to finite sky coverage effects, as discussed in Sec. V C.

relations in quadrature with inverse variance weighting. This should be a reasonable approximation to the sum in Eq. (57), as inverse-variance weighting tends to be dominated sharply by the lowest noise correlation. The results are shown in the left panel of Fig. 7. We see that broadly speaking (with some alternation as a function of L), the best sensitivity is achieved by EPIC, followed by SPTPol, ACTPol, Planck, Polarbear, WMAP, ACT, Spider, and SPT. Obviously any specific experimental concept will be outperformed by the CV case, as confirmed in the left panel of Fig. 7.

B. Signal-to-noise

Calling on Eq. (66), we compute the SNR expected for all the CMB experiments we consider as a function of the rms CIP fluctuation $\Delta_{\rm cl}$. The results are shown in the right panel of Fig. 7. Assuming a scale-invariant spec-

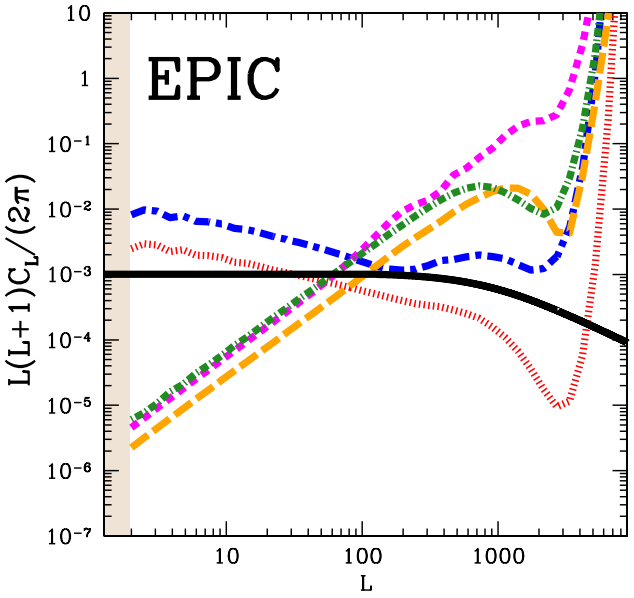

FIG. 5: Predicted noise power spectrum δC_L in the reconstructed CIP perturbation field Δ_{LM} for the proposed EPIC satellite, as a function of angular scale L. Colors (line-styles) are as in Fig. 3. We separately plot the noise for distinct pairs of observables: TT is shown as an orange (short-dash long-dashed), TE as a green (dot-dashed) line, EE as a magenta (short-dashed) line, BE as a blue (long-dashed) line, and BT as a red (dotted) line. Also shown (black solid line) is the power spectrum C_L^{Δ}, for a scale-invariant spectrum of CIPs with the maximum amplitude allowed by galaxy clusters. The beige (grey) shaded region shows the range of L that is not included in our estimates, due to finite sky coverage effects, as discussed in Sec. V C.

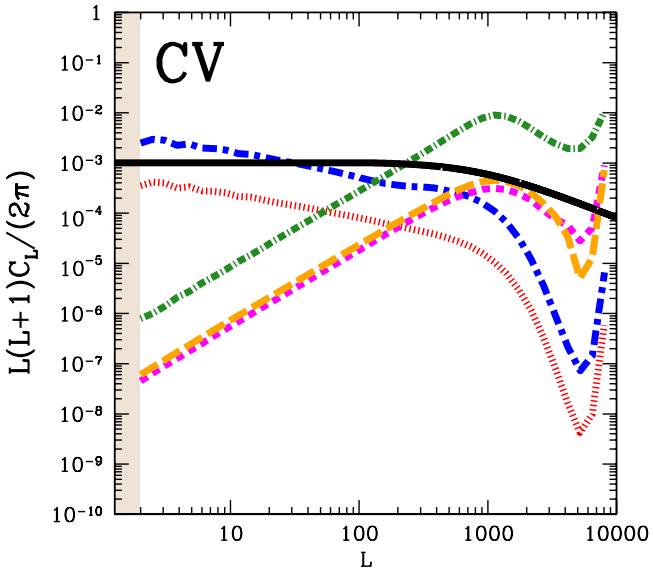

FIG. 6: Predicted noise power spectrum δC_L in the reconstructed CIP perturbation field Δ_{LM} for an ideal cosmic variance limited experiment, as a function of angular scale L. Colors (line-styles) are as in Fig. 3. We separately plot the noise for distinct pairs of observables: TT is shown as an orange (short-dash long-dashed), TE as a green (dot-dashed) line, EE as a magenta (short-dashed) line, BE as a blue (long-dashed) line, and BT as a red (dotted) line. Also shown (black solid line) is the power spectrum C_L^{Δ}, for a scale-invariant spectrum of CIPs with the maximum amplitude allowed by galaxy clusters. The beige (grey) shaded region shows the range of L that is not included in our estimates, due to finite sky coverage effects, as discussed in Sec. V C.

trum, we see that already with WMAP, we are able to probe compensated fluctuations in the baryon fraction of $\sim 10\%$, the lowest value probed in Ref. [35]. We define a 'detection' as a measurement with $S/N \geq 3$. Currently operating sub-orbital experiments, like SPT and ACT, and the upcoming Spider experiment, perform comparably to WMAP. Although these experiments are sensitive to a fairly large rms CIP amplitude, the cluster constraint was obtained at a different scale, and it is important to check the constraint using the independent probe offered by the CMB.

Planck and Polarbear offer the next major improvement in SNR, probing $\Delta_{\rm cl} \simeq 3\%$ and higher. The addition of polarization sensitivity to SPT and ACT lowers the range of detectable $\Delta_{\rm cl}$ to 0.6%. EPIC would be able to measure $\Delta_{\rm cl} \simeq 0.4\%$. This is a factor of 20 lower than the currently allowed maximum from measurements of the baryon fraction in galaxy clusters. In the CV case, an additional order of magnitude improvement in SNR is possible.

As discussed in Sec. V C, we conservatively estimated sensitivity, omitting low-L modes. In practice, all-sky experiments like WMAP, Planck, and EPIC could probe even smaller CIP amplitudes than estimated here, as the $L = 1$ mode could contribute significantly to the SNR. If experimental techniques improve (approaching the cosmic variance limit at very high l), and a way is found to disentangle CIPs from secondary CMB anisotropies at these high l, a further order of magnitude improvement in sensitivity is theoretically possible, using the estimators developed in this work. Additionally, we have been conservative in our estimates of SNR, assuming that only one useful frequency channel is available for EPIC. The mission concept actually calls for ~ 7 channels, in order to achieve good foreground subtraction. It may be that if EPIC is built, more than one useful channel of signal is obtained, improving the SNR by a factor of order unity.

It may be that CIPs are not an independent Gaussian random field (as assumed here), but rather, as in some curvaton models [34], correlated with the usual adiabatic fluctuations. In that case CIPs will induce 3-point correlations between CMB observables, through effects at decoupling. In future work, we will pursue the possibility of probing CIPs with the corresponding CMB bispectra.

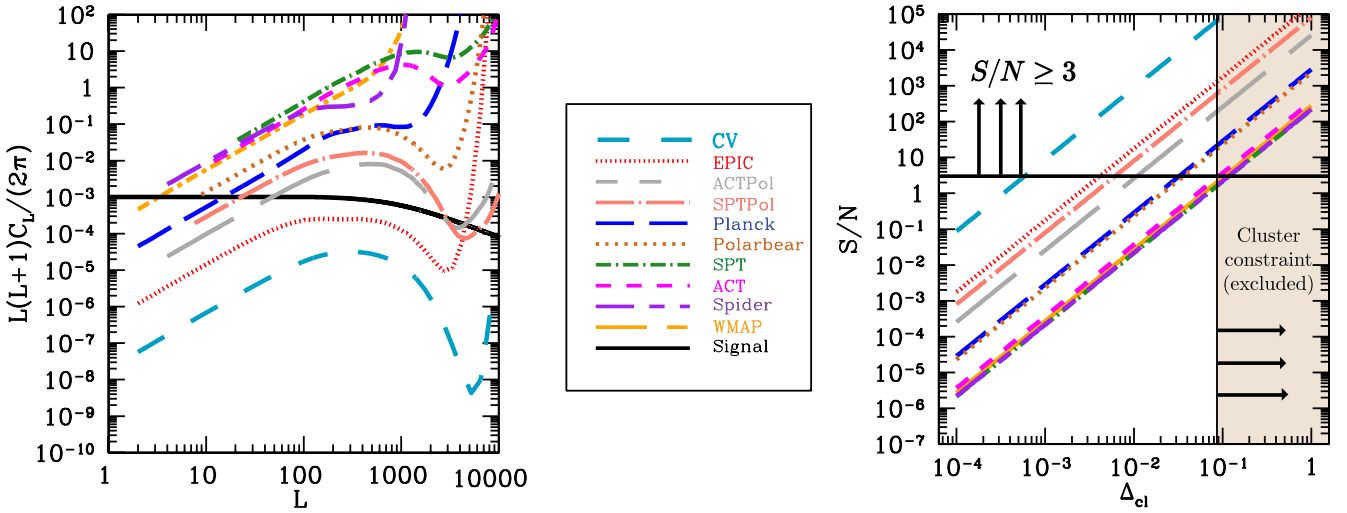

FIG. 7: Combined (predicted) noise power spectrum δC_L in the reconstructed CIP perturbation field Δ_{LM} for 9 different CMB experiments, as a function of angular scale L. Colors and line styles for each experiment are indicated in the legend (center). Here noise for the 5 different estimators (TT, TE, EE, BE, and BT) is added in quadrature. Noise curves terminate at L values where modes become inaccessible due to finite sky effects, as discussed in Sec. V C. Also shown (black solid line) is the power spectrum C_L^{Δ} , marked signal, for a scale-invariant spectrum of CIPs with the maximum amplitude allowed by galaxy clusters. The left panel shows predicted total errors for the indicated experiments. The right panel shows the predicted signal-to-noise ratio (SNR) that results from these errors, evaluated using Eq. (66), and assuming a scale-invariant spectrum of CIPs [evaluated using Eq. (47)]. The SNR is plotted as a function of the rms CIP fluctuation $\Delta_{\rm cl}$ on cluster scales. The range of fluctuations $\Delta_{\rm cl}$ excluded by cluster measurements [35] is shown as a beige (grey) band, bounded by a vertical black line with rightward pointing arrows. The black line with upward arrows attached shows the 'detection' region, defined by $S/N = 3$.

VII. CONCLUSIONS

Compensated isocurvature perturbations provide an intriguing empirical possibility for large-amplitude departures from homogeneity in the early Universe. The current constraint, $\lesssim 10\%$ to the amplitude of such perturbations is surprisingly weak. While Ref. [35] has pointed out that there may be CMB signatures induced by CIPs at reionization, we have shown here that the CMB effects of CIPs at the surface of last scatter would be several orders of magnitude larger. We then calculated the full two-point temperature/polarization correlations induced by CIPs on the CMB and developed the minimum-variance estimators for measuring the CIP field with the CMB.

The WMAP satellite may be sensitive to a scale-invariant spectrum of CIPs, but only if the CIP amplitude is close to its current upper bound. In the future, sensitivity to CIP amplitudes as small as $\sim 3\%$ may be achieved by instruments in operation and $\sim 0.1\%$-level fluctuations accessible in the near future with precise ground and space-based polarization experiments that are under construction (ACTPol and SPTPol) or in conceptual development (EPIC).

Many steps must be taken before such measurements can be implemented with real data. Techniques to deal with partial-sky coverage and realistic instrumental noise properties must be developed, but these techniques should be similar to those being developed already to measure the effects of weak gravitational lensing on the CMB. Likewise, techniques must be developed to distinguish the off-diagonal correlations induced by CIPs from those induced by weak gravitational lensing (e.g. [95]), which should be comparable in amplitude if the CIP field Δ is comparable to the lensing potential ϕ, i.e, $\sim 1\%$.

Although lensing is already included in our reconstruction noise estimates [σ_{Δ_L} in Eq. (57)], it might also induce bias in the reconstruction of the CIPs. Gravitational lensing of the CMB will induce correlations of similar form to Eqs. (53)-(54), with the distinction that the functions $S_{ll'}^{L,\rm XX'}$ will be different for lensing than for CIPs. In the case of lensing, these functions describe the remapping of CMB observables on a lensing-deflected sky. In the case of CIPs, these functions describe the detailed physical dependence of CMB anisotropies on the baryon density. If Eq. (57) is applied to the extension of Eqs. (53)-(54) that includes gravitational lensing, a bias will be induced in the measurement of Δ_{LM}.

The differing forms of $S_{ll'}^{L,\rm XX'}$ will allow lensing and CIPs to be disentangled. Using a straightforward generalization of the estimator in Eq. (57) that includes terms for both CIPs and lensing, the bias induced by lensing on CIP measurements may be removed, simultaneously reconstructing the lensing and CIP fields. This is analogous to the estimators discussed in Ref. [95], where it is shown that if reionization is patchy because of inhomogeneity in the distribution of ionized bubbles around the first sources, the contributions of patchy reionization

and lensing may be distinguished. In future work, we will explicitly compute the bias in CIP searches that will be induced by lensing, and will construct the estimators that disentangle lensing from CIPs. As in Ref. [95], we expect that the signal-to-noise of the biased and unbiased estimators should be nearly the same, and so gravitational lensing should not affect the signal-to-noise estimates of this paper.

The measurements we propose in this paper offer a precise test of how closely the primordial baryon and dark-matter distributions are matched and approach the CIP amplitudes allowed in curvaton models. Moreover, if future CMB experiments detect subdominant isocurvature fluctuations between matter and radiation, the techniques developed in this work could disentangle contributions from the baryon and CDM isocurvature modes. Even greater gains in sensitivity are theoretically possible if the cosmic-variance limit is approached at high l by future experiments. We are optimistic that in the near future, we will learn just how well baryons trace dark matter in the early Universe.

Acknowledgments

We acknowledge useful conversations with C. Chiang, C. Dvorkin, G. Holder, M. LoVerde, K. M. Smith, T. L. Smith, D. N. Spergel, and M. Zaldarriaga. We thank B. Jones and A. Fraisse for providing updated parameters for Spider forecasting. DG was supported at the Institute for Advanced Study by the National Science Foundation (AST-0807044), and is grateful for the hospitality of the Aspen Center for Physics, where part of this work was completed. MK thanks the support of the Miller Institute for Basic Research in Science and the hospitality of the Department of Physics at the University of California, where part of this work was completed. This work was supported at Caltech by DoE DE-FG03-92-ER40701, NASA NNX10AD04G, and the Gordon and Betty Moore Foundation. Part of the research described in this paper was carried out at the Jet Propulsion Laboratory, California Institute of Technology, under a contract with the National Aeronautics and Space Administration.

Appendix A: Tensors on the sphere

Here we review the tensor-spherical-harmonic formalism, following closely Ref. [86]. The metric on the 2-sphere is

$$g = \begin{pmatrix} 1 & 0 \\ 0 & \sin^2\theta \end{pmatrix}, \tag{A1}$$

where θ is the polar angle defined with respect to the origin of the orientation vector $\hat{n}$. It is useful to introduce the orthonormal basis

$$\hat{e}_\theta = \begin{pmatrix} 1 \\ 0 \end{pmatrix} \quad \hat{e}_\phi = \begin{pmatrix} 0 \\ \sin^2\theta \end{pmatrix}. \tag{A2}$$

The tensor spherical harmonics are [67]

$$Y^{\rm E}_{lm,ab} = \frac{N_l}{2}\left(Y_{lm:ab} - \frac{1}{2}g_{ab}Y^c_{lm:c}\epsilon^c_a\right), \tag{A3}$$

$$Y^{\rm B}_{lm,ab} = \frac{N_l}{2}\left(Y_{lm:ac}\epsilon^c_b + Y_{lm:bc}\epsilon^c_a\right), \tag{A4}$$

where the normalization constant is given by

$$N_l \equiv \sqrt{\frac{2\,(l-2)!}{(l+2)!}}, \tag{A5}$$

and all indices following ":" denote covariant derivatives taken on the 2-sphere. The indices l and m are multipole indices, while a and b are tensor indices.

Using Ref. [70], the covariant derivatives may be expressed in terms of spin-2 spherical harmonics [68, 70]:

$$Y_{lm:ab} = -\frac{l\,(l+1)}{2}Y_{lm}g_{ab} + \frac{1}{2}\sqrt{\frac{(l+2)}{(l-2)!}} \times \left[{}_2Y_{lm}\,(m_+ \otimes m_+) + {}_{-2}Y_{lm}\,(m_- \otimes m_-)\right]_{ab}. \tag{A6}$$

The left subscript "2" denotes a spin-weighted spherical harmonic ${}_sY_{lm}$ of spin s, while $\otimes$ denotes a tensor product. The spherical basis vectors $m_\pm$ are

$$m_\pm = \frac{1}{\sqrt{2}}\left(\hat{e}_\theta \mp i\hat{e}_\phi\right). \tag{A7}$$

In row-column form, the spherical tensor basis functions are then [86]

$$Y^{\rm E} = \frac{\begin{pmatrix} ({}_2Y + {}_{-2}Y) & i\sin\theta\,({}_{-2}Y - {}_{+2}Y) \\ i\sin\theta\,({}_{-2}Y - {}_{+2}Y) & -\sin^2\theta\,({}_{-2}Y + {}_{+2}Y) \end{pmatrix}}{2\sqrt{2}}, \tag{A8}$$

$$Y^{\rm B} = \frac{\begin{pmatrix} i\,({}_{+2}Y - {}_{-2}Y) & \sin\theta\,({}_{-2}Y + {}_{+2}Y) \\ \sin\theta\,({}_{-2}Y + {}_{+2}Y) & i\sin^2\theta\,({}_{-2}Y - {}_{+2}Y) \end{pmatrix}}{2\sqrt{2}}, \tag{A9}$$

where we have suppressed the lm indices for the sake of brevity.

To evaluate the polarization anistropies induced by CIPs (see Sec. III), it is useful to obtain identities for the product of two distinct (generally different l and m values) spherical harmonics. Using Eqs. (A8)–(A9), it

can be shown that [86]

$$\left(X^{\mathrm{E},ab}\right)^* Y^{\mathrm{E}}_{ab} = \frac{1}{2}\ \left({}_{+2}X^* \otimes {}_{+2}Y + {}_{-2}X^* \otimes {}_{-2}Y\right), \quad \text{(A10)}$$

$$\left(X^{\mathrm{B},ab}\right)^* Y^{\mathrm{E}}_{ab} = -\frac{i}{2}\ \left({}_{+2}X^* \otimes {}_{+2}Y - {}_{-2}X^* \otimes {}_{-2}Y\right), \quad \text{(A11)}$$

where X and Y signify tensor spherical harmonics on the left hand side of Eqs. (A10-A11) and the corresponding spin-weighted spherical harmonics on the right hand side of these equations. Relations such as these help express the integrals of Sec. III as integrals over 3 spin-weighted spherical harmonics. These are then evaluated by applying the relation [70]

$$\begin{aligned}&\int\ d\hat{n}\left({}_{s_1}Y^*_{l_1m_1}\right)\left({}_{s_2}Y_{l_2m_2}\right)\left({}_{s_3}Y_{l_3m_3}\right)\\ &=\ (-1)^{m_1+s_1}\sqrt{\frac{(2l_1+1)(2l_2+1)(2l_3+1)}{4\pi}}\\ &\times\ \begin{pmatrix} l_1 & l_2 & l_3\\ s_1 & -s_2 & -s_3\end{pmatrix}\begin{pmatrix} l_1 & l_2 & l_3\\ -m_1 & m_2 & m_3\end{pmatrix}.\end{aligned} \quad \text{(A12)}$$

In evaluating the contribution of terms proportional to $d^2f^{(0)}/d\Delta^2$ to perturbed LOS solutions for polarization anisotropies, integrals over four spin-weighted spherical harmonics must be evaluated. They may be simplified using the identity [96]

$$\begin{aligned}&{}_{-s}Y_{l''-m''} \otimes {}_{s}Y_{l'm'} = \sqrt{(2l''+1)(2l'+1)}\\ &\times \sum_{L''M''S''}(-1)^{M''+S''}\sqrt{\frac{2L''+1}{4\pi}}\,{}_{S''}Y_{L''M''}\\ &\times\begin{pmatrix} l'' & l' & L''\\ m'' & -m' & M''\end{pmatrix}\begin{pmatrix} l'' & l' & L''\\ -s & s & -S''\end{pmatrix}.\end{aligned} \quad \text{(A13)}$$

Appendix B: Derivative power spectra

We wish to estimate the derivatives $d^nX_l(k)/d\Delta^n$ of the transfer functions $X_l(k)$. For the first derivatives, we use a 5-point approximation, running CAMB [61] repeatedly to obtain the transfer functions at 5 different values of Ω_bh^2 and Ω_ch^2. The first derivative is then well approximated by

$$\frac{dX_l(k)}{d\Delta} = \sum_{i=-2}^{2}\frac{c_iX^i_l(k)}{12\Delta}. \quad \text{(B1)}$$

Here $X^i_l(k)$ denotes the transfer function evaluated under the transformation $\Omega_b \to \Omega_b(1+\Delta)$, $\Omega_c \to \Omega_c - \Delta\Omega_b$. We find that the choice $\Delta = 0.02$ works well to evaluate the first derivatives. We run convergence tests by doubling and halving Δ and find that $dX_l(k)/d\Delta$ has converged to $\sim 5\%$, which is more than sufficient for our purposes. We use values $c_0 = 0$, $c_{\pm1} = \pm8$, and $c_{\pm2} = \mp1$ [97].

For the second derivatives, we use the 7-point numerical approximation

$$\frac{d^2X_l(k)}{d\Delta^2} = \sum_{i=-3}^{3}\frac{c_iX^i_l(k)}{180\Delta^2}. \quad \text{(B2)}$$

In this case, we find that the choice $\Delta = 0.066$ lies comfortably in the zone of convergence. The corresponding coefficients are $c_0 = -490$, $c_{\pm1} = 270$, $c_{\pm2} = -27$, and $c_{\pm3} = 2$. We run convergence tests by doubling and halving Δ and find that $d^2X_l(k)/d\Delta^2$ has converged to $\sim 5\%$, which is accurate enough for the work presented here. The resulting derivative power spectra, defined by Eqs. (23), are shown in Figs. B1–B3. All derivative power spectra are computed using CAMB, with $\tau = 0$. These are then multiplied by a homogeneous reionization damping envelope with mean optical depth $\tau \simeq 0.086$, given by expressions in Ref. [98]. This was done to isolate the effects of patchy decoupling, screened by a homogeneous optical depth at reionization (with $z_{\mathrm{reion}} \simeq 10.5$), from additional (smaller) anisotropies induced at reionization.

Appendix C: Harmonic expansion of CMB transfer functions

The most convenient way to generalize Eq. (2) to include terms $\propto \Delta^2(\hat{n})$ is to derive second-order corrections to

$$f_{LM} \equiv \int d\hat{n}\, Y^*_{LM}(\hat{n}) f(\eta,\hat{n}). \quad \text{(C1)}$$

Using the Taylor expansion in real space defined by Eq. (8) and Eq. (C1), we obtain

$$\begin{aligned} f_{LM} &= f^{(1)}_{LM} + f^{(2)}_{LM} + ...,\\ f^{(1)}_{LM} &\equiv \Delta_{LM}\frac{df^{(0)}}{d\Delta},\\ f^{(2)}_{LM} &\equiv \frac{1}{2}\frac{d^2f^{(0)}}{d\Delta^2}\sum_{L'M',L''M''}\beta^{L''M''}_{L'M',LM}\Delta_{L'M'}\Delta^*_{L''M''},\end{aligned} \quad \text{(C2)}$$

where

$$\beta^{L''M''}_{L'M',LM} \equiv \xi^{L''M''}_{L'M',LM}K^{LM}_{L'M',L''M''}. \quad \text{(C3)}$$

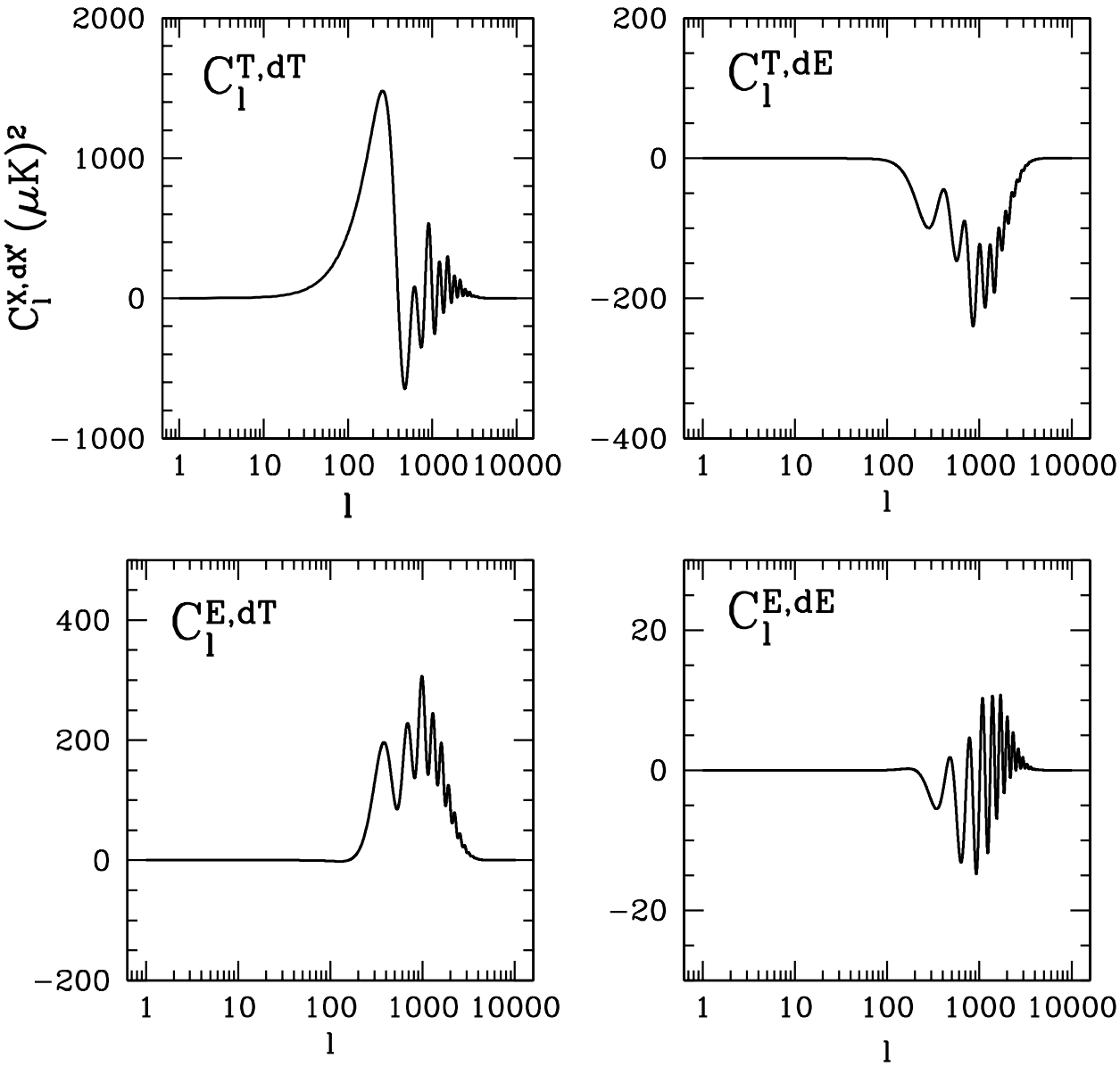

FIG. B1: Lowest-order first-derivative power spectra, as defined in Secs. II and III. These are necessary to reconstruct Δ_{LM}, as described in Sec. V. We use the numerical methods of Appendix B to obtain these curves using a modified version of the CAMB [61] code.

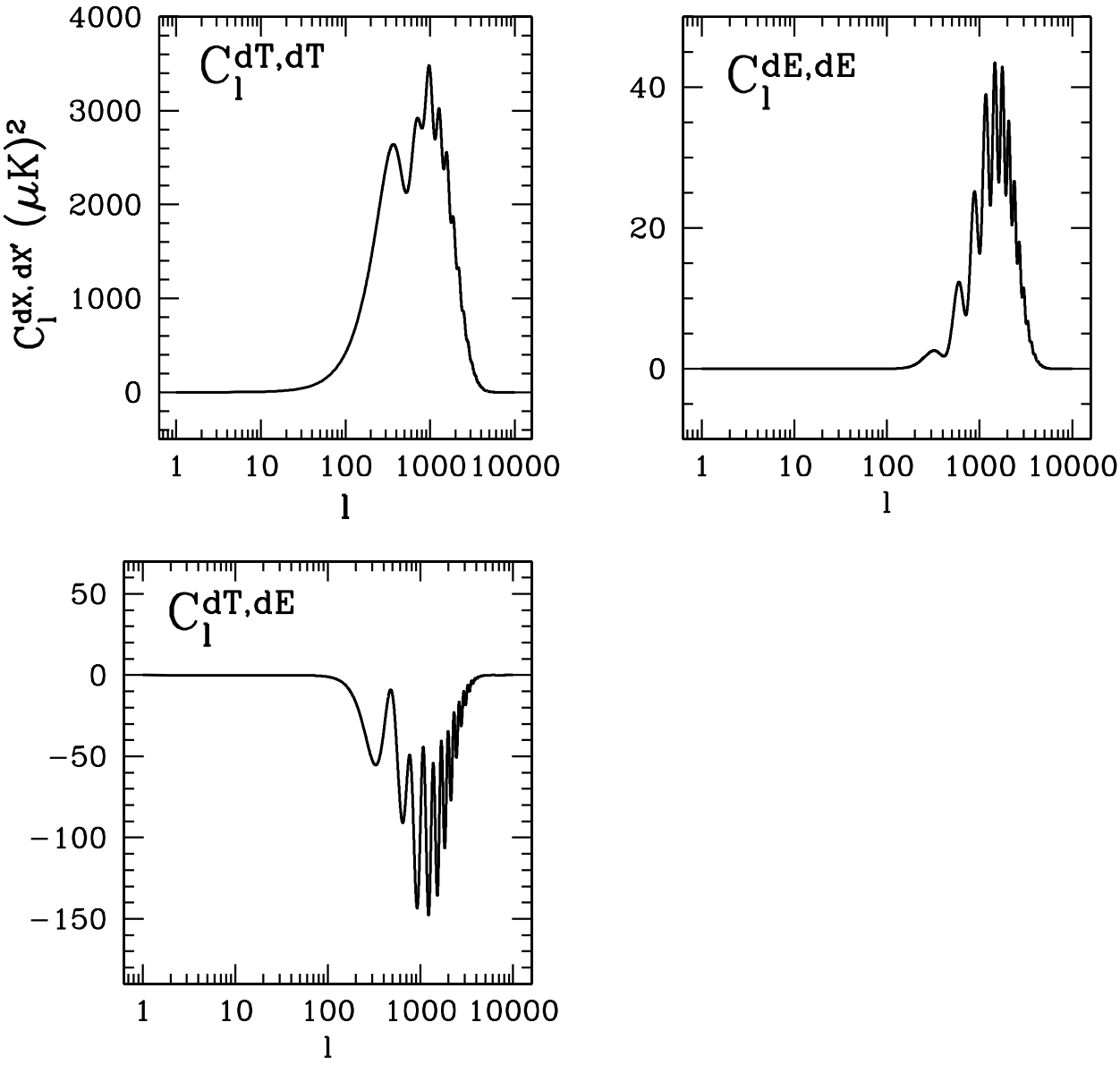

FIG. B2: Second-order first-derivative power spectra, as defined in Secs. II and III. These are necessary to estimate the corrected power spectra $C_l^{XX',(2)}$. We use the numerical methods of Appendix B to obtain these curves using a modified version of the CAMB [61] code.

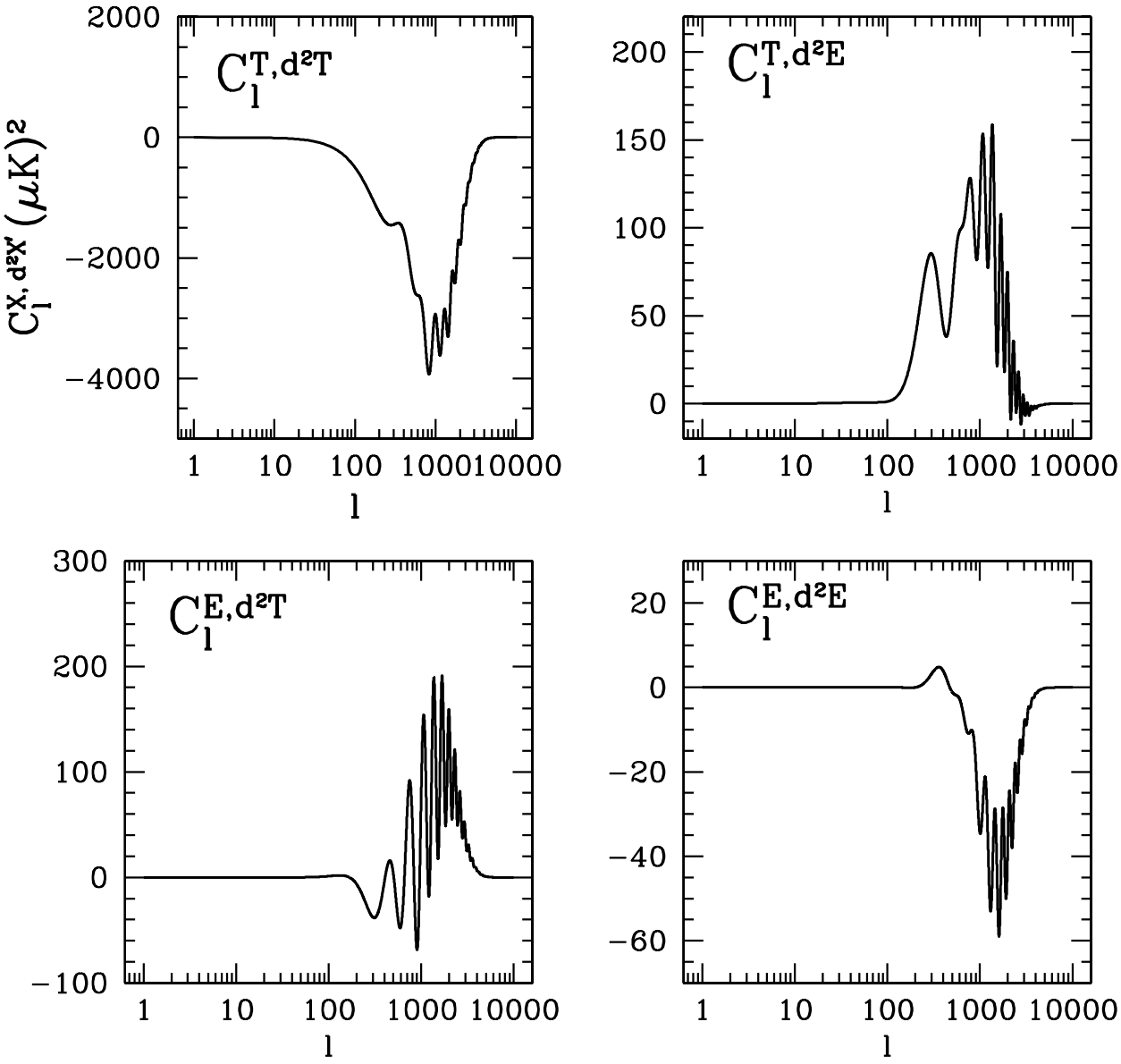

FIG. B3: Second-derivative power spectra, as defined in Secs. II and III. These are necessary to estimate the corrected power spectra $C_l^{\mathrm{XX}',(2)}$. We use the numerical methods of Appendix B to obtain these curves using a modified version of the CAMB [61] code.

[1] A. H. Guth and S. Pi, Phys.Rev.Lett. **49**, 1110 (1982).
[2] A. D. Linde, Phys.Lett. **B116**, 335 (1982).
[3] J. M. Bardeen, P. J. Steinhardt, and M. S. Turner, Phys. Rev. D **28**, 679 (1983).
[4] S. Hawking, Phys.Lett. **B115**, 295 (1982), revised version.
[5] V. F. Mukhanov and G. V. Chibisov, Sov. Phys. JETP. **83**, 475 (1982).
[6] A. A. Starobinsky, Phys. Lett. B. **117**, 175 (1982).
[7] D. Larson et al., Astrophys. J. Suppl. Ser. **192**, 16 (2011), arXiv:1001.4635.
[8] N. Padmanabhan et al., Mon. Not. R. Astron. Soc. **378**, 852 (2007), arXiv:astro-ph/0605302.
[9] M. Tegmark et al., Astrophys. J. **606**, 702 (2004), arXiv:astro-ph/0310725.
[10] R. H. Brandenberger, Int. J. Mod. Phys. A **9**, 2117 (1994), arXiv:astro-ph/9310041.
[11] A. D. Linde, Sov. Phys. JETP. **40**, 1333 (1984).
[12] A. Linde and V. Mukhanov, Phys. Rev. D **56**, 535 (1997), arXiv:astro-ph/9610219.
[13] V. F. Mukhanov, H. A. Feldman, and R. H. Brandenberger, Phys. Rep. **215**, 203 (1992).
[14] M. Axenides, R. Brandenberger, and M. Turner, Phys. Lett. B. **126**, 178 (1983).
[15] D. Langlois and A. Riazuelo, Phys. Rev. D **62**, 043504 (2000), arXiv:astro-ph/9912497.
[16] D. Langlois, Phys. Rev. D **59**, 123512 (1999), arXiv:astro-ph/9906080.
[17] P. J. E. Peebles, Astrophys. J. **510**, 523 (1999), arXiv:astro-ph/9805194.
[18] P. J. E. Peebles, Astrophys. J. **510**, 531 (1999), arXiv:astro-ph/9805212.
[19] S. D. Burns, ArXiv Astrophysics e-prints (1997), arXiv:astro-ph/9711303.
[20] D. Seckel and M. S. Turner, Phys. Rev. D **32**, 3178 (1985).
[21] W. Hu, Phys. Rev. D **59**, 021301 (1999), arXiv:astro-ph/9809142.
[22] W. Hu, E. F. Bunn, and N. Sugiyama, Astrophys. J. Lett. **447**, L59+ (1995), arXiv:astro-ph/9501034.
[23] K. Enqvist, H. Kurki-Suonio, and J. Väliviita, Phys. Rev. D **62**, 103003 (2000), arXiv:astro-ph/0006429.
[24] K. Enqvist and H. Kurki-Suonio, Phys. Rev. D **61**, 043002 (2000), arXiv:astro-ph/9907221.
[25] E. Komatsu et al., Astrophys. J. Suppl. Ser. **192**, 18 (2011), arXiv:1001.4538.
[26] J. Väliviita and T. Giannantonio, Phys. Rev. D **80**, 123516 (2009), arXiv:0909.5190.
[27] C. Zunckel, P. Okouma, S. Muya Kasanda, K. Moodley, and B. A. Bassett, Physics Letters B **696**, 433 (2011), arXiv:1006.4687.
[28] M. Bucher, J. Dunkley, P. G. Ferreira, K. Moodley, and C. Skordis, Phys. Rev. Lett. **93**, 081301 (2004), arXiv:astro-ph/0401417.
[29] M. Kawasaki and T. Sekiguchi, Progress of Theoretical Physics **120**, 995 (2008), arXiv:0705.2853.
[30] M. Beltrán, J. García-Bellido, J. Lesgourgues, and M. Viel, Phys. Rev. D **72**, 103515 (2005), arXiv:astro-ph/0509209.
[31] U. Seljak, A. Slosar, and P. McDonald, JCAP. **10**, 14 (2006), arXiv:astro-ph/0604335.
[32] M. Beltrán, J. García-Bellido, J. Lesgourgues, and A. Riazuelo, Phys. Rev. D **70**, 103530 (2004), arXiv:astro-ph/0409326.
[33] T. Takahashi, M. Yamaguchi, and S. Yokoyama, Phys. Rev. D **80**, 063524 (2009), arXiv:0907.3052.
[34] C. Gordon and J. R. Pritchard, Phys. Rev. D **80**, 063535 (2009), arXiv:0907.5400.
[35] G. P. Holder, K. M. Nollett, and A. van Engelen, Astrophys. J. **716**, 907 (2010), arXiv:0907.3919.
[36] C. Gordon and A. Lewis, Phys. Rev. D **67**, 123513 (2003), arXiv:astro-ph/0212248.
[37] A. Lewis and A. Challinor, Phys. Rev. D **76**, 083005 (2007), arXiv:astro-ph/0702600.
[38] R. Barkana and A. Loeb, Mon. Not. R. Astron. Soc. **363**, L36 (2005), arXiv:astro-ph/0502083.
[39] M. Kawasaki, T. Sekiguchi, and T. Takahashi, arXiv: (2011), 1104.5591.
[40] K. Sigurdson, A. Kurylov, and M. Kamionkowski, Phys. Rev. D **68**, 103509 (2003), arXiv:astro-ph/0306372.
[41] A. Lewis and A. Challinor, Phys. Rep. **429**, 1 (2006), arXiv:astro-ph/0601594.
[42] The Planck Collaboration (2006), arXiv:astro-ph/0604069.
[43] M. D. Niemack et al., in *Society of Photo-Optical Instrumentation Engineers (SPIE) Conference Series* (2010), vol. 7741 of *Presented at the Society of Photo-Optical Instrumentation Engineers (SPIE) Conference*, arXiv:1006.5049.
[44] C. Dvorkin and K. M. Smith, Phys. Rev. D **79**, 043003 (2009), arXiv:0812.1566.
[45] J. J. McMahon et al., in *American Institute of Physics Conference Series*, edited by B. Young, B. Cabrera, & A. Miller (2009), vol. 1185 of *American Institute of Physics Conference Series*, pp. 511–514.
[46] J. Bock et al. (EPIC Collaboration) (2009), 0906.1188.
[47] D. H. Lyth, C. Ungarelli, and D. Wands, Phys. Rev. D **67**, 023503 (2003), arXiv:astro-ph/0208055.
[48] S. Gupta, K. A. Malik, and D. Wands, Phys. Rev. D **69**, 063513 (2004), arXiv:astro-ph/0311562.
[49] K. Enqvist, S. Nurmi, G. Rigopoulos, O. Taanila, and T. Takahashi, JCAP. **11**, 3 (2009), arXiv:0906.3126.
[50] D. E. Kaplan, M. A. Luty, and K. M. Zurek, Phys.Rev. **D79**, 115016 (2009), 0901.4117.
[51] M. R. Buckley and L. Randall (2010), arXiv:1009.0270.
[52] R. Allahverdi, B. Dutta, and K. Sinha, Phys. Rev. D **83**, 083502 (2011), arXiv:1011.1286.
[53] P. Gu, M. Lindner, U. Sarkar, and X. Zhang, Phys. Rev. D **83**, 055008 (2011).
[54] J. J. Heckman and S. Rey (2011), arXiv:1102.5346.
[55] J. McDonald (2010), arXiv:1009.3227.
[56] D. Grin, O. Doré, and M. Kamionkowski (2011), arXiv:1107.1716.
[57] E. Bertschinger (1995), arXiv:astro-ph/9506070.
[58] U. Seljak and M. Zaldarriaga, Astrophys. J. **469**, 437 (1996), arXiv:astro-ph/9603033.
[59] C. Ma and E. Bertschinger, Astrophys. J. **455**, 7 (1995), arXiv:astro-ph/9506072.
[60] M. Zaldarriaga and D. D. Harari, Phys. Rev. D **52**, 3276 (1995), arXiv:astro-ph/9504085.
[61] A. Lewis and A. Challinor, Phys. Rev. D **66**, 023531 (2002), arXiv:astro-ph/0203507.

[62] L. Senatore, S. Tassev, and M. Zaldarriaga, JCAP. **9**, 38 (2009), arXiv:0812.3658.

[63] L. Senatore, S. Tassev, and M. Zaldarriaga, JCAP. **8**, 31 (2009), arXiv:0812.3652.

[64] R. Khatri and B. D. Wandelt, Phys. Rev. D **79**, 023501 (2009), arXiv:0810.4370.

[65] S. Dodelson, *Modern cosmology* (Academic Press, Amsterdam, 2003).

[66] D. A. Varshalovich, A. N. Moskalev, and V. K. Khersonsky, *Quantum theory of angular momentum: irreducible tensors, spherical harmonics, vector coupling coefficients, 3nj symbols.* (Singapore: World Scientific (1988) 514p., 1988).

[67] M. Kamionkowski, A. Kosowsky, and A. Stebbins, Phys. Rev. D **55**, 7368 (1997), arXiv:astro-ph/9611125.

[68] M. Zaldarriaga and U. Seljak, Phys. Rev. D **55**, 1830 (1997), arXiv:astro-ph/9609170.

[69] C. Dvorkin, W. Hu, and K. M. Smith, Phys. Rev. D **79**, 107302 (2009), arXiv:0902.4413.

[70] W. Hu, Phys. Rev. D **62**, 043007 (2000), arXiv:astro-ph/0001303.

[71] T. Okamoto and W. Hu, Phys. Rev. D **67**, 083002 (2003), arXiv:astro-ph/0301031.

[72] J. Silk, Astrophys. J. **151**, 459 (1968).

[73] L. Pogosian, A. P. S. Yadav, Y.-F. Ng, and T. Vachaspati (2011), 1106.1438.

[74] W. Hu, Astrophys. J. **529**, 12 (2000), arXiv:astro-ph/9907103.

[75] D. Baumann, A. Cooray, and M. Kamionkowski, New Astron. **8**, 565 (2003), astro-ph/0208511.

[76] O. Doré, G. Holder, M. Alvarez, I. T. Iliev, G. Mellema, U.-L. Pen, and P. R. Shapiro, Phys. Rev. D **76**, 043002 (2007), arXiv:astro-ph/0701784.

[77] A. Lewis, Phys. Rev. D **78**, 023002 (2008), arXiv:0804.3865.

[78] U. Seljak, Astrophys. J. **463**, 1 (1996), arXiv:astro-ph/9505109.

[79] M. Zaldarriaga and U. Seljak, Phys. Rev. D **58**, 023003 (1998), arXiv:astro-ph/9803150.

[80] M. Zaldarriaga, Phys. Rev. D **62**, 063510 (2000), arXiv:astro-ph/9910498.

[81] U. Seljak and M. Zaldarriaga, Phys. Rev. D **60**, 043504 (1999), arXiv:astro-ph/9811123.

[82] A. Hajian and T. Souradeep, Astrophys. J. Lett. **597**, L5 (2003), arXiv:astro-ph/0308001.

[83] A. Hajian and T. Souradeep, arXiv (2005), arXiv:astro-ph/0501001.

[84] A. R. Pullen and M. Kamionkowski, Phys. Rev. D **76**, 103529 (2007), arXiv:0709.1144.

[85] M. Kamionkowski, Phys. Rev. Lett. **102**, 111302 (2009), arXiv:0810.1286.

[86] V. Gluscevic, M. Kamionkowski, and A. Cooray, Phys. Rev. D **80**, 023510 (2009), arXiv:0905.1687.

[87] A. P. S. Yadav, R. Biswas, M. Su, and M. Zaldarriaga, Phys. Rev. D **79**, 123009 (2009), arXiv:0902.4466.

[88] R. R. Caldwell et al. (2011), arXiv:1104.1634.

[89] L. Knox, Phys. Rev. D **52**, 4307 (1995), arXiv:astro-ph/9504054.

[90] H. V. Peiris et al., Astrophys. J. Suppl. Ser. **148**, 213 (2003), arXiv:astro-ph/0302225.

[91] The Polarbear Collaboration, arXiv: (2010), 1011.0763.

[92] B. P. Crill et al., in *Society of Photo-Optical Instrumentation Engineers (SPIE) Conference Series* (2008), vol. 7010 of *Presented at the Society of Photo-Optical Instrumentation Engineers (SPIE) Conference*, arXiv:0807.1548.

[93] S. Das et al., Astrophys. J. **729**, 62 (2011), arXiv:1009.0847.

[94] E. Shirokoff et al. (2010), arXiv:1012.4788.

[95] M. Su et al. (2011), arXiv:1106.4313.

[96] W. Hu and M. White, Phys. Rev. D **56**, 596 (1997), arXiv:astro-ph/9702170.

[97] P. Henrici, *Elements of Numerical Analysis.* (New York: John Wiley, 336p., 1964).

[98] W. Hu and M. White, Astrophys. J. **479**, 568 (1997), arXiv:astro-ph/9609079.